Earth-Science Reviews 153 (2016) 274–300

Contents lists available at ScienceDirect

Earth-Science Reviews

journal homepage: www.elsevier.com/locate/earscirev

From the highest to the deepest: The Gaoping River–Gaoping Submarine Canyon dispersal system

James T. Liu [a,*], Ray T. Hsu [a], Jia-Jang Hung [a], Yuan-Pin Chang [a], Yu-Huai Wang [a], Rebecca H. Rendle-Bühring [b], Chon-Lin Lee [c], Chih-An Huh [d], Rick J. Yang [a]

[a] Department of Oceanography, National Sun Yat-sen University, Kaohsiung 80424, Taiwan ROC
[b] Department of Geosciences, University of Bremen, PO Box 330440, D-28334 Bremen, Germany
[c] Department of Marine Environment, National Sun Yat-sen University, Kaohsiung 80424, Taiwan ROC
[d] Institute of Earth Sciences, Academia Sinica, Taipei, 11529, Taiwan ROC

ARTICLE INFO

Article history:
Received 2 September 2014
Received in revised form 22 September 2015
Accepted 27 October 2015
Available online 30 October 2015

Keywords:
Small mountainous river
Submarine canyon
Typhoon
River flood
Hyperpycnal flow
Turbidite
Terrestrial sediment
Hemipelagic sediment

ABSTRACT

There are many different source-to-sink dispersal systems around the world, and the Gaoping River (GPR)–Gaoping Submarine Canyon (GPSC) provides an example especially as a canyon-captured system. The GPR, a small mountainous river having an average gradient of 1:150, and the GPSC, which links the river catchment to the deep-sea basin, represent two major topographic features around SW Taiwan. Together, they constitute a terrestrial-to-marine dispersal system that has an overriding impact on the source-to-sink transport of sediment in this region. The GPSC extents from the mouth of the GPR through the shelf and slope and into the northeastern Manila Trench, a distance of about 260 km. It is a major conduit for the transport of terrestrial sediment and carbon to the South China Sea and the landward transport of particles of marine and biological origin.

In the GPSC the dominant mode of suspended-sediment transport is tidal oscillations and the net direction is up-canyon. In contrast, sediment transport associated with episodic gravity-driven events is down-canyon. The steady sedimentation of the tidal regime results in hemipelagic mud across the canyon floor, whereas the gravity-driven (hyperpycnal) regime causes turbidite erosion and deposition along the canyon thalweg.

Typhoon-induced river floods often lead to hyperpycnal plumes at the river mouth, which directly and indirectly ignite hyperpycnal turbidity currents in the canyon forming an effective agent for transporting large amounts of terrestrial organic material (modern and fossil carbon) to the South China Sea basin. Therefore, the GPR–GPSC represents a source-to-sink system in which terrestrial sediment in a mountainous catchment is promptly removed and transported to the deep sea by episodic gravity flows. This is also a pathway by which modern terrestrial organic carbon is quickly and effectively delivered to the deep sea.

Contents

* Corresponding author.
E-mail address: james@mail.nsysu.edu.tw (J.T. Liu).

http://dx.doi.org/10.1016/j.earscirev.2015.10.012
0012-8252/

1. Introduction

In a sediment-routing system the erosion of mountainous regions and the final deposition are linked when the sediment is moved from its source to its sink (Allen, 2008). Globally the amount of sediment delivered to the oceans by rivers is influenced by tectonic processes, which control the topography along the sediment-routing system, and by the climate, which controls the weathering and erosion in river catchments (Allen, 2008).

There is a great diversity of sediment-routing systems in the world, which have a range of source and sink characteristics on continental margins (Walsh and Nittrouer, 2009). There are numerous examples including systems on passive continental margins such as the Po River (Fox et al., 2004; Traykovski et al., 2007), the Amazon River (Nittrouer and DeMaster, 1996), the Mississippi River (Bianchi and Allison, 2009), the Yangtze River (Changjiang), and the Yellow River (Huanghe). Some of these systems form active deltas (Bianchi and Allison, 2009; Saito et al., 2001; Wu et al., 2007). Examples on active continental margins include the Ganges-Brahmaputra River (Goodbred, 2003), and the Eel River (Warrick, 2014). Along the Pacific Rim there are small mountainous rivers on high standing islands, such as the Lanyang, Zhuoshui, and Gaoping in Taiwan (Liu et al., 2009b, 2013) and the Waipaoa River in New Zealand (Kuehl et al., in this volume; Marsaglia et al., 2010; Parra et al., 2012). A great majority of these rivers flow into a bay or a gulf and wide or narrow shelves. There is another kind of sediment-routing system that includes river-associated submarine canyons (Baker and Hickey, 1986; Choi and Wilkin, 2007; Hsu et al., 2014; Lopez-Fernandez et al., 2013; Palanques et al., 2005; Walsh and Nittrouer, 2009), which comprise only 2.62% of all the 4025 submarine canyons in the world (Harris and Wihteway, 2011). Most of these submarine canyons are separated from their associated river mouths by a portion of the continental shelf (Liu and Lin, 2004). Only in rare cases does the submarine canyon head reach into or very near the mouth of the river, such as the Sepik River (Kineke et al., 2000), the Biobio River (Sobarzo et al., 2001), and the Gaoping River (GPR) (Liu et al., 2002).

Among all the river dispersal systems, the Gaoping is particularly interesting because there is a strong coupling between the dynamics that move the sediment and the sediment record in the system that links the catchment of a mountainous river and a submarine canyon on an active tectonic setting. The characteristics of this sediment-routing system makes it an ideal natural laboratory to study source-to-sink processes and responses across the boundaries of different environmental units within short time and space scales.

Based on topographic features, the Gaoping sediment dispersal system in southern Taiwan is geographically divided into three segments (Fig. 1A), each with its own source-to-sink implications: 1) the southern part of the Taiwan orogen (Fig. 1B); 2) the tectonically active drainage basin of the GPR which includes the Gaoping coastal plain; 3) the Gaoping Submarine Canyon (GPSC) that extends from the mouth of the GPR into the NE corner of the South China Sea basin, which is fronted by the steep slope of Taiwan Strait to the north (Yu et al., 2009).

This paper reviews the three key segments of the GPR–GPSC system and discuss their influence on the form and function of this dispersal system. The emphasis is on the process–response linkages between sediment processes and the associated geochemical signals carried by fine-grained sediment through the system.

2. Background

2.1. System morphology

The GPR is the largest river in Taiwan in terms of drainage area (3257 km^2) and the second largest in terms of suspended-sediment load (49 MT per year) (Liu et al., 2009a) (Fig. 2A). The headwater of the GPR is located in the southern part of the Central Range near Mt. Jade (Yu-Shan) whose elevation is 3952 m above sea level (Fig. 2B). It is a small mountainous river, with 48% of its drainage basin above 1000 m, 32% between 100 and 1000 m, and 20% below 100 m (Liu et al., 2009a). Consequently, the riverbed gradient is 1:15 in the upper reaches, 1:100 in the middle reaches, and 1:1000 in the lower reaches, with an average of 1:150 (Fig. 2C, Liu et al., 2009a).

Located ~1 km from the mouth of the GPR, the head of the GPSC cuts across the narrow Gaoping shelf and slope, and merges into the northern end of the Manila Trench about 260 km away (Yu et al., 2009, Fig. 1C). The morphology of the canyon is closely affected by the intrusions of mud diapers in the upper reaches and thrust faulting in the middle and lower reaches of the canyon (Chiang and Yu, 2006). High and steep walls characterize the head region of the canyon (Yu et al., 1993). The canyon has relief exceeding 600 m, with a cross-sectional geometry varying from V-shaped to broadly U-shaped +/− irregular troughs (Chiang and Yu, 2006, 2011). The formation of this submarine canyon was controlled by the tectonic evolution of the arc-continent collision between the Chinese continental margin and the Luzon volcanic arc, which generated many structural deformations in the Taiwan accretionary wedge, including the GPSC (Liu et al., 1997).

2.2. Strong forcing: typhoons and earthquakes

In addition to tectonic deformation, typhoons and earthquakes are two major factors that affect the system (Liu et al., 2013). On average, approximately four typhoons pass through Taiwan per year (Liu et al., 2013). Among the historical typhoons, 23% were from the western Pacific Ocean, and 13% were from the SCS (Liu et al., 2013). Typhoons can affect the system when still hundreds of kilometers away by bringing marine-sourced foraminifera into the upper reaches of the GPSC.

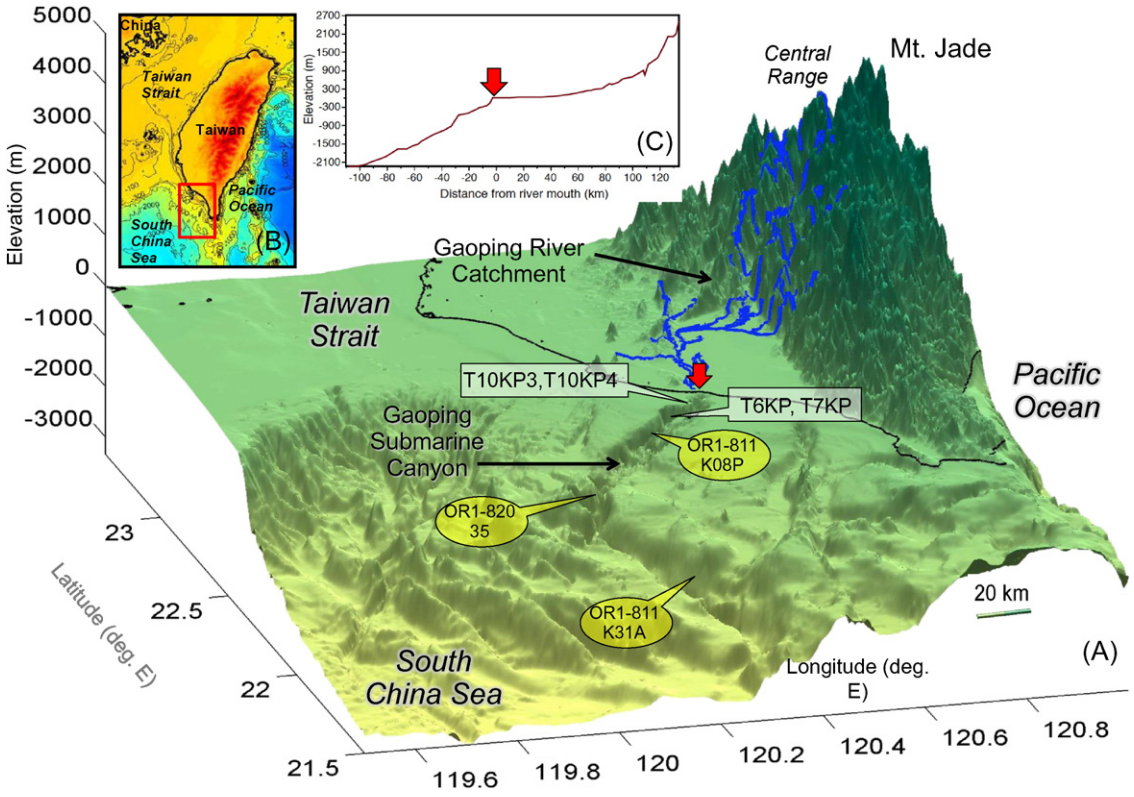

Fig. 1. A 3-D topographic map of the GPR basin and the upper and middle reaches of the GPSC (A). The smaller map of Taiwan shows the area included in the 3-D map (B). The topographic changes from near the mountainous source area to the middle reaches of the canyon are shown by the plot of elevations along the thalweg of the river and the submarine canyon (C). The red arrow indicates the confluence point of the river and submarine canyon. The deployment locations of four sediment trap moorings (T6KP, T7KP, T10KP3, T10KP4) discussed in the text are indicted. The locations of three long piston cores (OR1-811 K08P, OR1-820 35, OR1-811 K31A) discussed in the text are also indicated.

During the proximal phase, when typhoons induce river floods, high waves and storm surges are typically present in the coastal areas and locally sourced sediments from the river flood and sea-floor resuspension dominate the sediment fluxes in the system (Liu et al., 2006). Typhoons are a significant factor not only as a geological agent that affects sediment generation and burial throughout the system on millennium time scales and longer, but also as a major forcing agent moving sediment from the terrestrial river catchment to the deep sea via the submarine canyon on time scales of hours and days (Liu et al., 2012; Hsu et al., 2014). This review considers how several recent typhoons, including Kalmaegi (2008), Morakot (2009), and Fanapi (2010) affected the source-to-sink processes in the GPR–GPSC system (Liu et al., 2013).

The influence of earthquakes has been minor in the sub-aerial GPR catchment area in recorded history compared to other areas in Taiwan. However, a major earthquake in 2006 triggered significant gravity flows in the nearby Fangliao Submarine Canyon and the lower GPSC and Manila Trench (Hsu et al., 2008; Carter et al., 2012; Su et al., 2012). Associated with the event, ~22 subsea communication cables were broken, implying the tremendous power of the gravity flows. Hung and Ho (2014) reported elevated concentrations and inventories of suspended matter and trace metals in both Fangliao and Gaoping canyons after this earthquake, which could be caused by the earthquake-triggered gravity flows.

2.3. A highly perturbed GPR catchment: complex signal generation

Landsides/debris flows triggered by earthquakes and typhoons episodically increase the sediment supply from upland catchments in the GPR drainage basin (Hsieh and Chyi, 2010; Liu et al., 2013). Fan terraces are a very common landscape form at the confluences of the major and secondary tributaries along the Qishan and Laonong Rivers (Hsieh and Chyi, 2010; Hsieh and Capart, 2013), and the stratigraphic sequences of these fans attest to the mass-wasting process that erode the mountains and aggrade the river channels and riverbanks (Hsieh and Chyi, 2010). An event that took place <200 yr BP, for example, caused the riverbed to elevate 120 m (Hsieh and Capart, 2013). Because of the episodic nature of the mass wasting, both the aggradation and subsequent incision progress rapidly, on time scales of less than a few hundred years (Hsieh and Chyi, 2010). There is recurring aggradation-incision in the history of tributary-fan development throughout the upper and middle-reaches of the GPR catchment, thus the high spatial and temporal variability in river morphology indicates that sedimentation to and in the river is dynamic and complex. Although typhoons and earthquakes are key driving forces in the sediment supply (Liu et al., 2013), there are other factors such as aggradation-incision that controls the 'fluvial behavior' of each tributary (Hsieh and Chyi, 2010; Hsieh and Capart, 2013). These in turn, form internal sources and sinks on centennial to millennium time scales within the river basin.

In 5–10 August 2009, a super typhoon (Morakot) hit Taiwan (Chien and Kuo, 2011). In about three days, it brought cumulative precipitation of 1677 mm in the GPR basin, which is equivalent to the annual rainfall in an ordinary year (Tsou et al., 2011). A catastrophic landslide in the upper reaches of the Qishan River on 9 August buried the Xiaolin Village and caused more than 400 casualties (Supplemental Fig. S1A). The Xiaolin Village was located at the foot of an ancient colluvium deposit that had accumulated over 120 m thick (Hsieh et al., 2012) (Supplemental Fig. S1B). The erosion left a concave-shaped slope (Supplemental Fig. S1C). Underlying the erosional slope of the Xiaolin landslide, the prevailing appearance (dated 21, 14.9, 13.7 and 12.0 ka) of mass-wasting sequences thicker than 20 m also suggests frequent recurrences of landslides/debris flows in this area (Hsieh et al., 2012), which would episodically generate enormous amount of sediment in the source-to-sink system.

Another more common type of disturbance brought on by typhoons on the time scale of days, is flooding of in the Gaoping fluvial plain south of the confluence of the Qishan, Laonong, and Ailiao rivers (Fig. 2B). River floods often cause erosion of the topsoil and destructions of man-made structures. For example during Typhoon Morakot, five of the nine bridges crossing the GPR were destroyed (Supplemental Fig. S2A, B). River dikes collapsed in many places, roads were washed away, and buildings were destroyed. Disturbances in the GPR affected

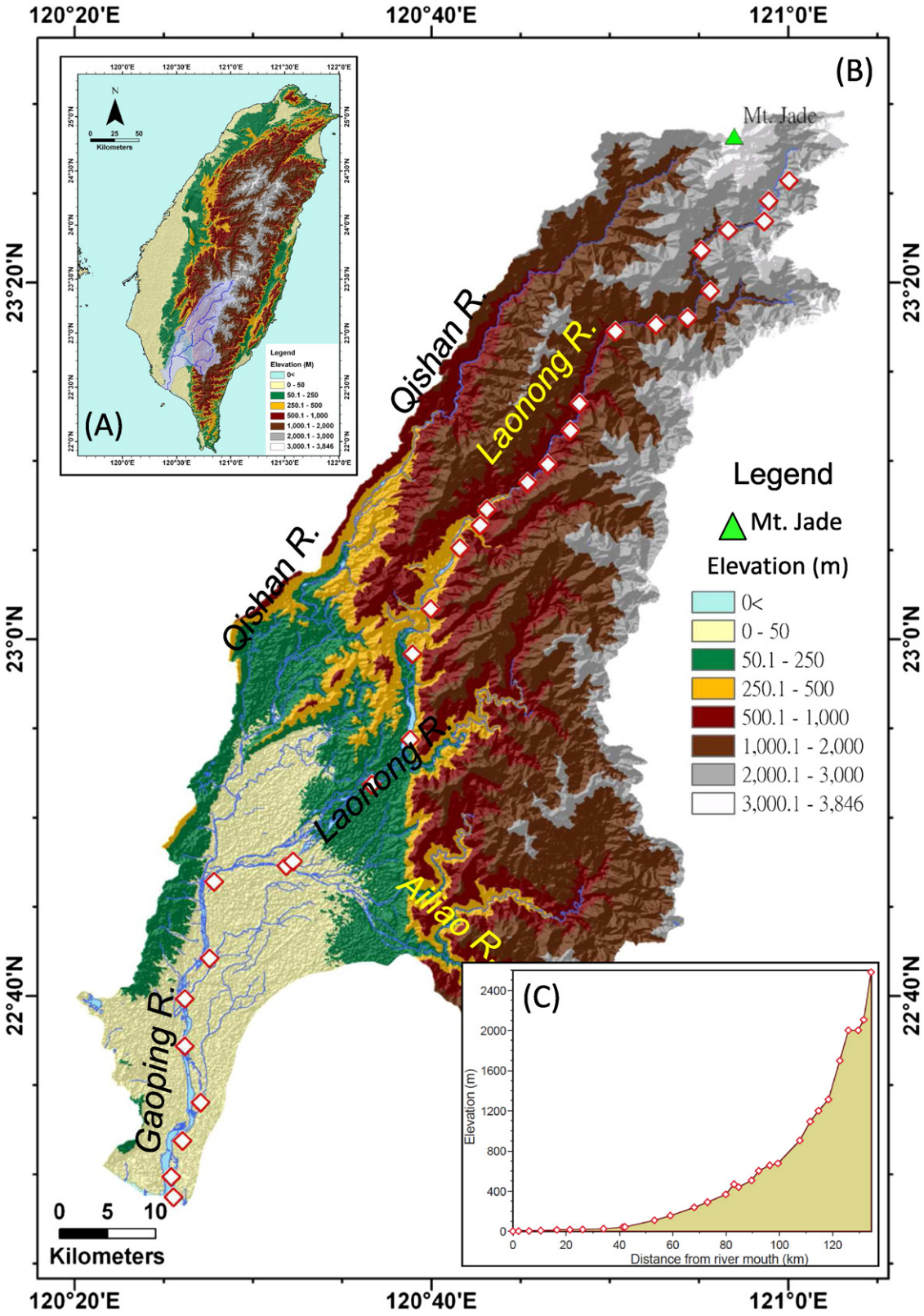

Fig. 2. (A) The topographic map of Taiwan showing the area of the GPR basin (grey). (B) An enlarged topographic map of the GPR basin, showing the main course of the GPR and the three major tributaries: Qishan River, Laonong River, and Ailao River. The diamond symbols show the locations of the elevations plotted in (C) along the thalweg of the main course of the river system. The source area is near Mt. Jade, the highest peak of the Central Range.

the characteristics of the fluvial sediment signal during the floods (Liu et al., 2013), which will be elaborated on in later Sections 4.1.2 and 5.4.

2.4. An effective conduit for land-sea exchanges: the Gaoping Submarine Canyon

The sediment discharged by the GPR to the open shelf and slope accounts for less than 20% of the river's sediment load (Huh et al., 2009a). A larger amount of the sediment is carried by gravity flows, in the form of hyperpycnal turbidity currents, via the GPSC, to the deeper South China Sea (Carter et al., 2012; Huh et al., 2009b; Liu et al., 2006, 2012, this volume). Polycyclic aromatic hydrocarbon (PAH) concentrations and compositional patterns show that riverine particulates are mostly directed to the NW-shelf and/or the GPSC (Fang et al., 2007). The GPSC also acts as a major sink for riverine trace metals (Hung and Hsu, 2004; Liu et al., 2009b). But studies show that the GPSC is actually a two-way conduit for land-sea exchanges of water masses and suspended particles (Liu et al., 2002, 2006; Liu and Lin, 2004; Lin et al., 2005). While terrigenous material is transported down the canyon towards the deep sea by gravity flows, marine-sourced biogenic material is transported landward via the canyon conduit by tide-dominated processes (Lin et al., 2005). Nevertheless, lithogenic sediments dominate suspended particles in the head region of the canyon (Liu et al., 2009b).

3. Approach and methods

The objectives of field monitoring and analysis of water and sediment in the GPR–GPSC system are firstly to address diversity in the source (terrestrial vs. marine), origin (lithogenic vs. biogenic), and history (modern vs. fossil) of the sediment. Consequently multiple geochemical and isotopic analyses were used to extract the geochemical characteristics (e.g., organic material, trace metals) of the sediment. Furthermore, tracers that can identify the origin of particles, such as biomarkers, PAHs, and foraminifers were used. $^{210}Pb_{ex}$ was employed as an indictor of steady settling in sediment in cores and sediment trap samples on the centennial time scale, and the AMS ^{14}C was used to determine the longer chronology of material in sediment cores and particles captured in non-sequential sediment traps.

Secondly, to address relationships between physical forcing and sediment responses, instrumented taut-line moorings were configured with CTDs, current meters, and sediment traps. To establish the coupling between processes in the water column and the seabed, mooring deployments were accompanied by water-column sampling of the suspended-sediment and concentrations, by sampling of the surficial sediment on the seafloor, and by coring at the deployment site. Concurrently, the hydrography at the deployment site was surveyed over tidal cycles. Results from eight mooring deployments are included in this review.

4. The environmental units in the Gaoping River–Gaoping Submarine Canyon system

4.1. The fluvial system

4.1.1. Hydrological cycles and episodic events

Due to the influence of typhoons and the monsoon climate, rainfall in the GPR basin is highly seasonal, most of which (70%) occurs during the flood season from June to September (Huh et al., 2009a; Milliman and Kao, 2005). Consequently, 91% of the annual discharge occurs in the flood season (Liu et al., 2002). Typhoon-related episodes of high runoff are accompanied by larger suspended-sediment discharge (Liu et al., 2013). Based on a 41-year long monthly discharge record, the temporal fluctuations of river runoff show important periodicities of about less than 12 years, 1 year, and 0.5 years. The 12-yr periodicity is close to the 11-yr cyclicities in the solar activities that affect decadal global climatic patterns in precipitation (Prokoph et al., 2012; Wang and Su, 2013). The monsoon climate, on the other hand, brings distinct dry and flood seasons over the annual hydrological cycle. The passing of typhoons mostly occurs in the summer and early fall, potentially bringing massive rainfall.

4.1.2. Sediment generation and delivery

The geology, topography, climate, and human activities in the river catchment lead to significantly higher physical and chemical weathering rates than the world average (Hung et al., 2004). Studies show that the sediment yield from the GPR basin (15 kg/m^2/yr) is higher than Taiwan's overall average (10 kg/m^2/yr) (Dadson et al., 2003), and much higher than the mean value of global small mountainous rivers (3 kg/m/yr) (Milliman and Syvitski, 1992). The rate of chemical erosion in the GPR basin is estimated to be 1.3 kg/m^2/yr, which is also much higher than the world average of 33–40 g/m^2/yr (Hung et al., 2004). During the flood season, on average, the river runoff and the sediment load are two to three orders of magnitude higher than those observed in the dry season, respectively (Hung et al., 2004). In general, the river discharges high sediment loads and strong geochemical signals to the sea in the flood season and during typhoon events.

The transport and delivery of sediment particulate C, N, and biomarkers differs substantially between dry and flood seasons. During the flood season, episodic floods from heavy monsoon rains or typhoons critically influence not only the annual load of the suspended-sediment but also POC and PN values. The concentrations of POC (PN) are closely correlated ($r > 0.92$, $p < 0.003$) with suspended-sediment concentrations, which in turn are dependent on water discharge during the flood season. This implies that they have the same source (Hung et al., 2012). The daily river transport of POC is estimated to be 5.98×10^6 g C/d in the dry season and $1.25–276 \times 10^6$ g C/d in the flood season. In 2007, the estimated annual load of suspended-sediment, POC and PN (based on discharge-weighted concentration) were 3.7×10^7 metric tons/yr, 226 Gg C/yr and 15 Gg N/yr, respectively (Hung et al., 2012). In the very dry year of 2002, the estimated suspended-sediment, POC and PN load were 2.14×10^6 metric tons/yr, 9.51 Gg C/yr and 1.53 Gg N/yr, respectively (Hung, unpublished data). Therefore, the load of river-borne materials in any particular year depends highly on the river discharge, which in turn, largely depends on the occurrence of typhoons in that year.

In the flood season, the suspended-sediment load was largely composed of the 10–63 μm fraction except possibly during an event. For example during Typhoon Pabuk, the 63–153 μm fraction dominated the suspended-sediment load. The grain-size distribution of POC generally matches that of suspended-sediment. However, during Typhoons Wutip and Sepat, the 63–153 and 2.7–10 μm fractions dominated the suspended-sediment load, probably representing the two pathways of POC in the GPR basin (Hung et al., 2012). As noted elsewhere, the coarse-grained fraction of POC, >25 μm in the case of the Eel River and >63 μm in the case of the Amazon River, is derived mainly from plant debris. The fine-grained fraction of POC, <4 μm in the case of the Eel River and <63 μm in the case of the Amazon River, is derived from the soil (Blair et al., 2003). Similar relationships are expected in the GPR basin.

Based on linear regression analyses, Liu et al. (2009a) found that of the five grain-size classes in suspension in the lower GPR (>500, 250–500, 63–250, 10–63, and 1.2–10 μm), all except for the >500 μm grain-size class are carriers of POC and PN in the surface water, with

Fig. 3. The sampling sites and sample types for biomarkers in two seasons are marked and color-coded in (A) and (B). Seasonal mean distribution patterns of carbon numbers derived from *n*-alkanes (C15–C35) of sediment and soil samples in (C) summer (flood season), and (D) winter (dry season). The mean compositions of carbon numbers are distinctive among the rock, agricultural soil, and suspended particles (E). The calculated Carbon Predominance Index (CPI) along the GPR in (F) summer and (G) winter, respectively (0 km is located at the river mouth).

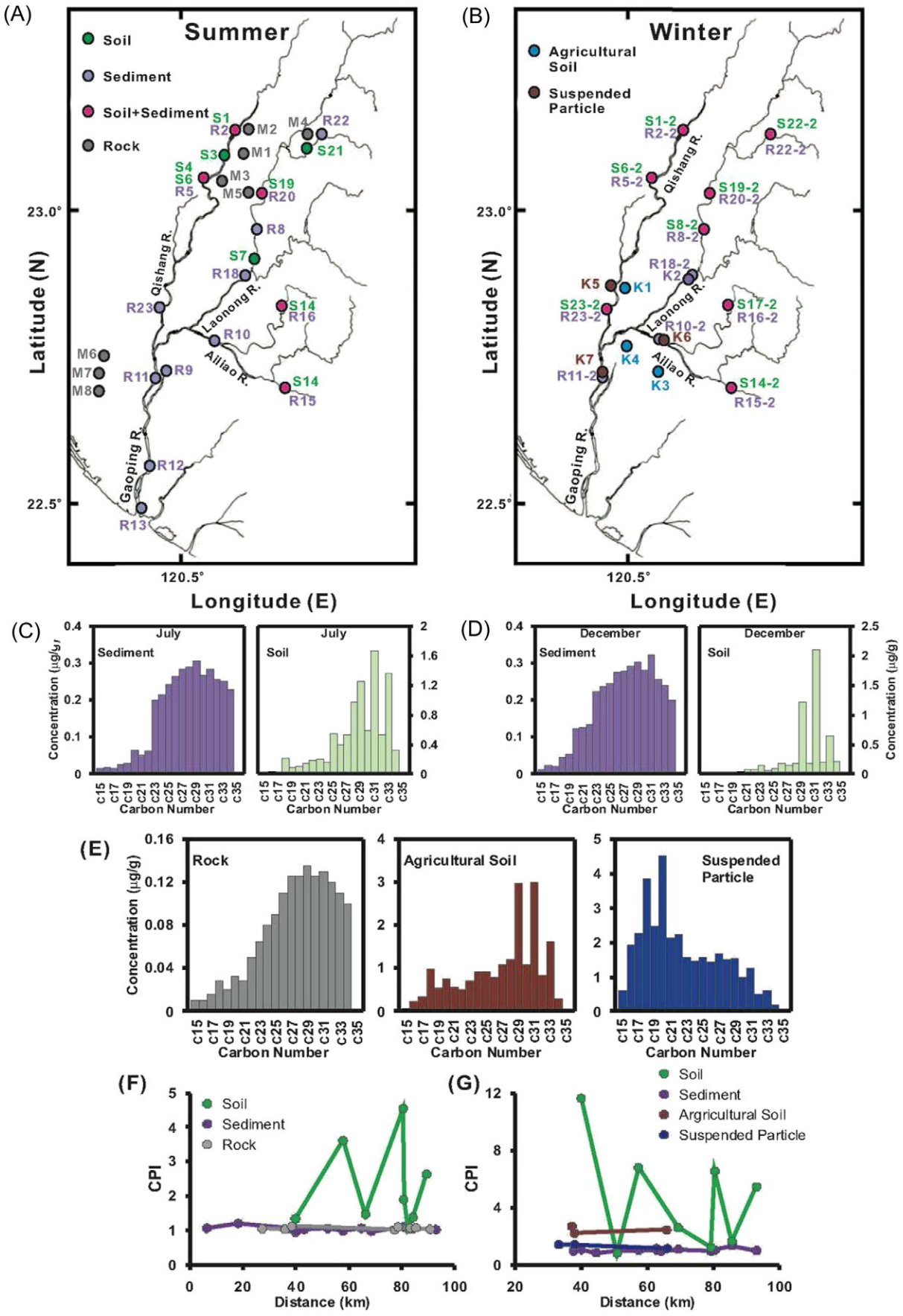
(A)
Summer
Soil
Sediment
Soil+Sediment
Rock
Qishang R.
Laonong R.
Alliao R.
Gaoping R.
Latitude (N)
Longitude (E)
23.0°
22.5°
120.5°
(B)
Winter
Agricultural Soil
Suspended Particle
(C)
July
Sediment
Soil
Concentration (μg/g)
Carbon Number
(D)
December
(E)
Rock
Agricultural Soil
Suspended Particle
(F)
CPI
Distance (km)
(G)

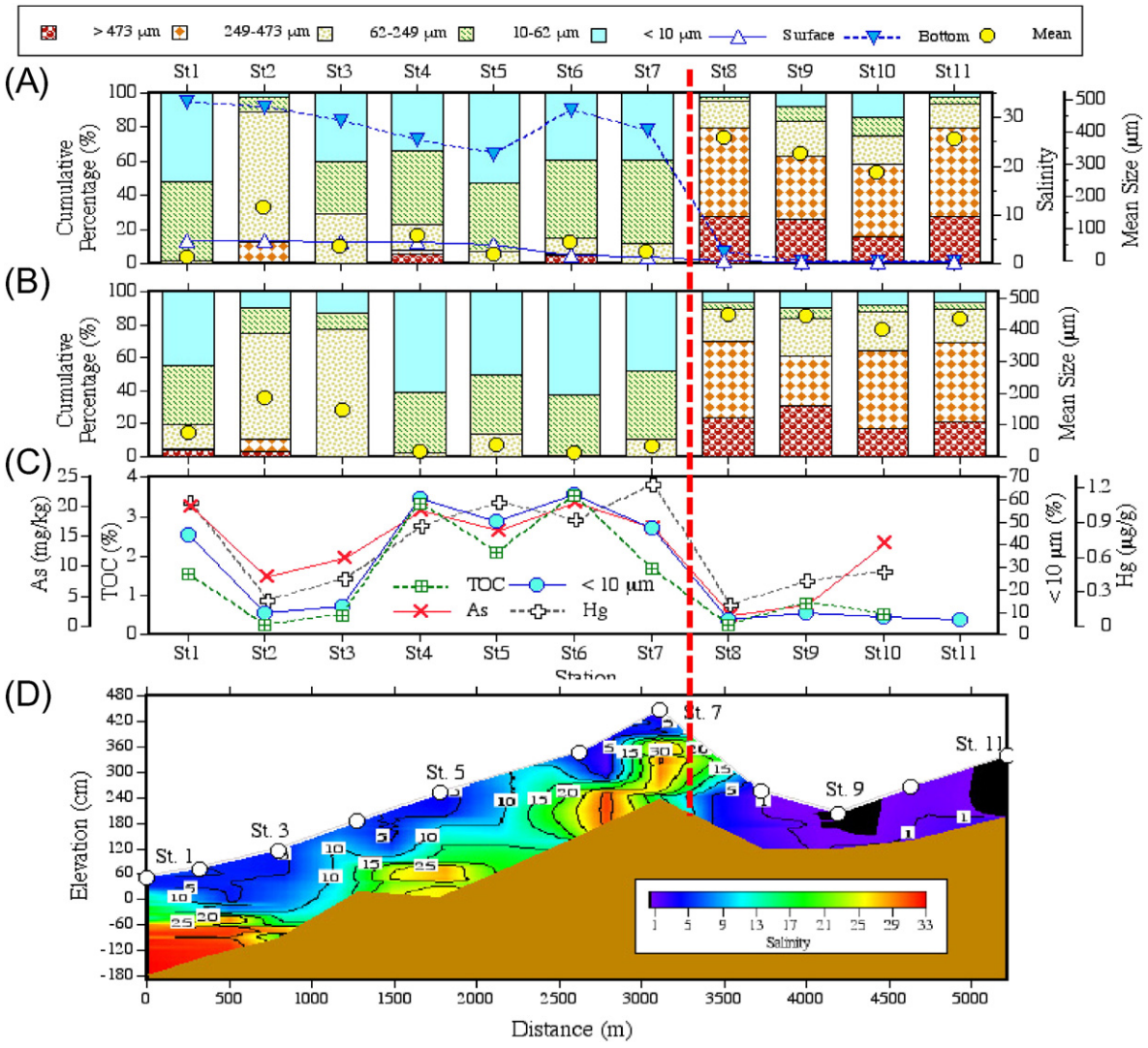

Fig. 4. Salt-wedge influence on sediment dynamics as shown by the along-channel grain-size composition of the unaltered riverbed sediment (A), the lithogenic fraction of the riverbed sediment, (C) the distribution of the medium-silt fraction and TOC, As, and Hg, and (D) the salinity structure that shows the boundary of the salt-wedge intrusion. The red dashed line indicates the boundary between the salt-wedge and fluvial regimes (taken from Liu et al., 2009a).

clearly terrestrial POC and PN in the 63–250, 10–63, and 1.2–10 μm size classes. In contrast, in the near-bed water, only the finest size class (1.2–10 μm) carries terrestrial POC and PN. On the riverbed, the coarsest size-classes of the total and lithogenic part of the sediment >473 and 249–473 μm are terrestrial. The finest two size-classes of <10 and 10–63 μm are of marine origin. These findings indicate that under non-typhoon conditions the GPR is exporting large-sized suspended terrestrial organic particles to the sea in the surface water and importing fine-grained marine organic particles as a result of estuarine circulation, potentially trapping these materials on the riverbed (see next section).

Under typhoon conditions, landslides and erosion of forested hill slopes in the GPR basin release large amount of woody debris in the form of driftwood that ranges from tree trunks to branches and twigs (Liu et al., 2013). Thus the driftwood is another pathway for modern terrestrial organic carbon (OC) to escape to the sea (Liu et al., 2012, 2013).

Hilton et al. (2011a) used biomarkers to distinguish the POC sources in the highly disturbed GPR basin, and found that they are mainly derived from bedrock erosion. Fifty-four samples including riverbed sediment, forest soil, agricultural soil, suspended particles, and rocks, were taken from the GPR basin in dry and flood seasons for biomarker studies (Fig. 3A,B). The mean distributions of carbon numbers derived from *n*-alkanes (C15–C35) show clear distinction between the sediment and soil in different seasons (Fig. 3C, D). In forest soil samples, similar to agricultural soil (Fig. 3E), the odd-number carbons are predominantly in higher molecular *n*-alkanes, meaning that hydrocarbons in the soil are mainly generated by vascular plants with less degradational influence (Fig. 3C, D). However, in riverbed sediment, there is no odd-number predominance, and the patterns are similar to those of rock samples (Fig. 3E). This discrepancy between the soil and river sediment is caused by different contributing sources, e.g. recently produced material (soils, standing biomass, and modern woody debris) and fossil OC (Sparkes et al., 2015). Thus, soil apparently contains fresh organic carbon from vascular plants (Brassell et al., 1986; Eglinton and Hamilton, 1967), whereas riverbed sediment is composed of reworked organic carbon (petrogenic alkanes). The carbon number composition of the riverine suspended particles suggests high dilution from degraded hydrocarbons released from sedimentary rocks by incision and landslides (Hilton et al., 2011b). Such petrogenically-sourced alkanes are predominant in sediments in the GPR basin and in suspended particles in the GPR.

The Carbon Predominance Index (CPI) indicates the 'freshness' of the OC. Larger values of CPI (usually >4) denote fresh and well-preserved *n*-alkanes with less diagenetic change and a smaller content from petrogenic sources (Powell et al., 1978; Powell and Mokirdy, 1973). On the other hand, petrogenic input and recycled organic matter (OM) have a CPI value close to unity (Pendoley, 1992). Along the GPR, the spatial distribution of CPI reveals that petrogenic hydrocarbons dominate river sediments regardless of the season (Fig. 3F, G). Therefore, there is a disassociation between the biomarkers in the soil and in the river sediment throughout the GPR system due to the overwhelming signals from the recycled OC sources in the system. This will be further discussed in 4.4.

4.2. The estuary

4.2.1. The estuarine filter related to the salt-wedge

In the flood season, tidally driven salt-water intrusion is the major factor influencing the hydrodynamics of the lower reaches of the GPR, which in turn, affects the down-river and water-column distribution of suspended and riverbed sediments (Liu et al., 2009a). The intrusion front of the salt-wedge driven by the tide creates a dynamic barrier (Fig. 4). On its landward side, the riverbed substrate is composed of sediment mostly coarser than 249 μm. Within the salt-wedge the riverbed substrate is finer, consisting mostly of mud (<63 μm) as in other systems (Bianchi, 2007; Carlin et al., 2015; Verlaan, 2000). The barrier creates a filter on the riverbed immediately seaward of the intrusion front, trapping higher percentages of clay-sized sediment and associated TOC and metal species (Figs. 4, 5, Hung et al., 2009; Liu et al., 2009a). The estuarine filter also separates the OM of terrestrial and marine sources in the suspended and riverbed sediments. Within the salt-wedge the major contributor of riverbed TOC is clay-sized marine sediment carried upstream by the intruding seawater (Fig. 5). The terrestrial POC is a minor contributor to the riverbed TOC.

4.2.2. Flocculation

Liu et al. (2009a) attribute the coarse-grained composition of the riverbed sediment immediately landward of the salt-wedge to the effect of flocculation (Fig. 5). The grain-size changes between riverbed and suspended-sediments are coupled. The abundances of most suspended and riverbed sediments in matching size-classes have a reciprocal relationship (negative feedback) through resuspension and deposition at the sediment-water interface. Only the grain-size classes of 62–473 μm on the riverbed and that of 63–250 μm in suspension are positively co-varying (both increase and decrease together) (Liu et al., 2009a). Unlike other grain-size classes in suspension and on the riverbed, this grain-size class has no statistically significant correlation with the salinity, suggesting it is neither marine nor terrestrial (Liu et al., 2009a). It consists largely of a transient floc population that is formed and destroyed over the course of a tidal cycle. Additionally as part of the same study, but not presented in Liu et al. (2009a), peak values of both the concentration and the mean grain size of the suspended sediment at the river mouth were found to coincide with minimum values in salinity. This suggests the presence of short-lived flocs during the ebbing tide when the salinity was the lowest, which corroborates well with the presence of the floc group.

4.3. The Gaoping Submarine Canyon

The collision between the continental margin of the northern South China Sea (part of the Eurasian plate) with the Luzon volcanic arc (Hsu and Sibuet, 2004; Lallemand and Tsien, 1997) has had significant influence on the seafloor structure and topography, including the formation of the GPSC (Liu et al., 1997). The collision area today is an accretionary prism/wedge (Chemenda et al., 2001; Huang et al., 1997) or an underfilled foreland basin (Yu, 2004), where sediments from the Taiwan orogen accumulate.

Both structural and sedimentary processes have affected the geomorphology of the GPSC (Chiang and Yu, 2006). In the upper sinuous part of the canyon, intrusions of mud diapirs have complicated the cut-and-fill process and have strongly affected the canyon morphology (Fig. 6). In the middle and lower reaches of the canyon, thrust faulting created two prominent bends in the course of the canyon (Fig. 1). Base tilting has also affected the morphology of the lower canyon (Chiang and Yu, 2006).

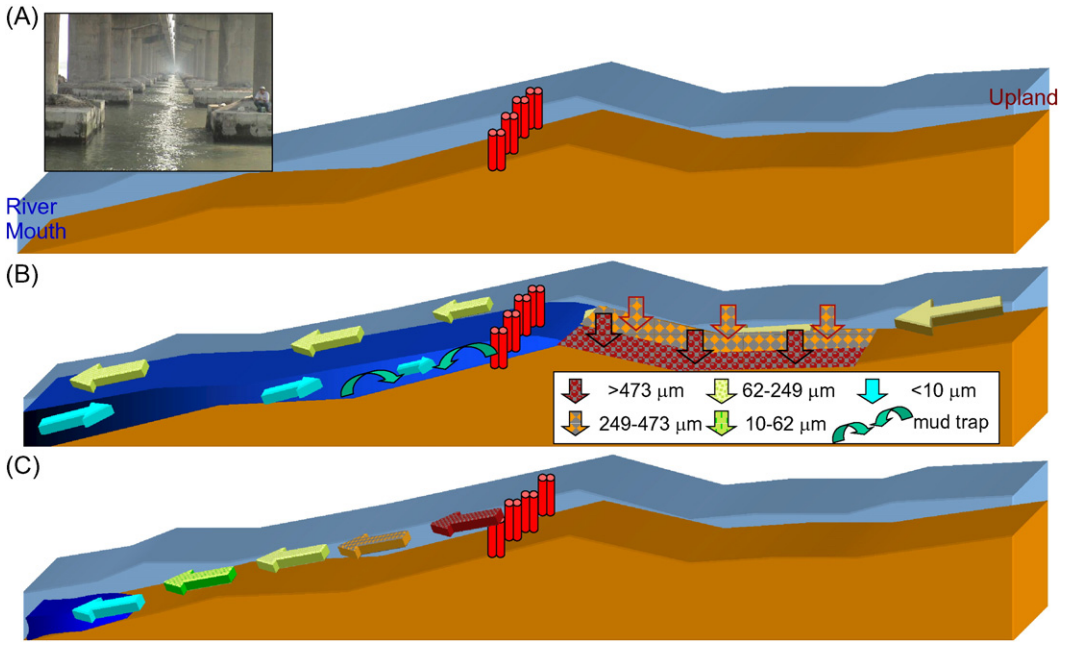

Fig. 5. Schematic 3-D plots of the river-salt wedge dynamics. (A) The basic setting showing the steep slope of the riverbed and the shallow water depth. The red columns represent the double pilings of the Xuangyuan Bridge (insert). (B) During flood, the river water slides over the intruding salt-wedge with little mixing. The landward end of the salt-wedge forms a dynamic barrier that facilitates the deposition of coarse sediment on its landward side and the trapping of fine-grained sediment on its seaward side (the estuarine filter). (C) During ebb, the salt-wedge withdraws to the river mouth, and river-borne sediments are transported to the sea relatively unimpeded.

Based on geomorphology and seismic surveys, Chiang and Yu (2008) hypothesized that gravity flows were the main control in the formation and maintenance of meanders of the canyon. For example, the sinuosity of the upper reaches of the canyon was likely caused by erosion of the seafloor due to gravity flows and slumping of the canyon walls (Fig. 6B, C, D, E), which could also trigger gravity flows. Identified boulders on the canyon floor in a 3-D image from multi-beam bathymetric surveys (Fig. 6D) support the presence of gravity flows (Shanmugam, 2006). Additionally, in a distal meander of the canyon, overspilled sediments at the outer bend of levees and a terrace of flat stratified facies at the inner bend also suggest active sedimentary processes in the canyon (Chiang and Yu, 2008, 2011).

4.3.1. Physical oceanography of the canyon

A branch of Kuroshio Current flows NW parallel to the coast through this area, bringing water masses and marine substances from the Pacific and the South China Sea (Liu et al., this volume). The observed temperature-salinity properties at the head region of the GPSC shows that the canyon is filled with three types of waters: 1) the effluent from the GPR, 2) Kuroshio Current water, and 3) South China Sea

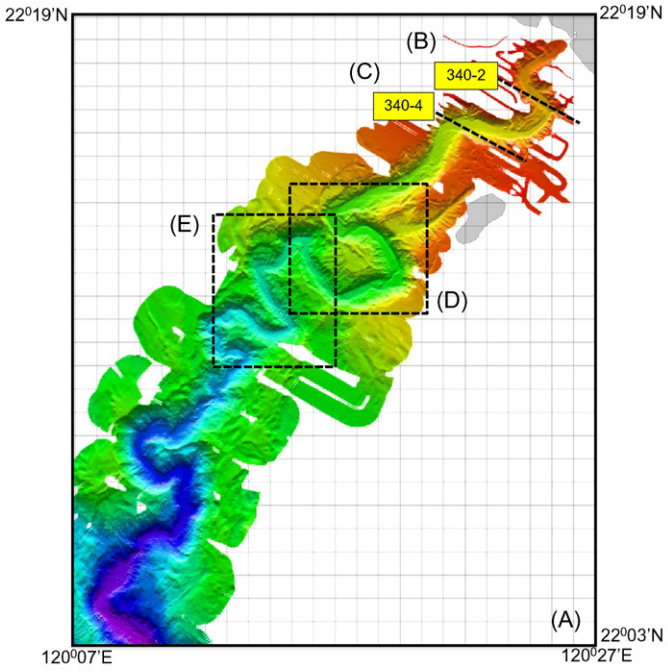

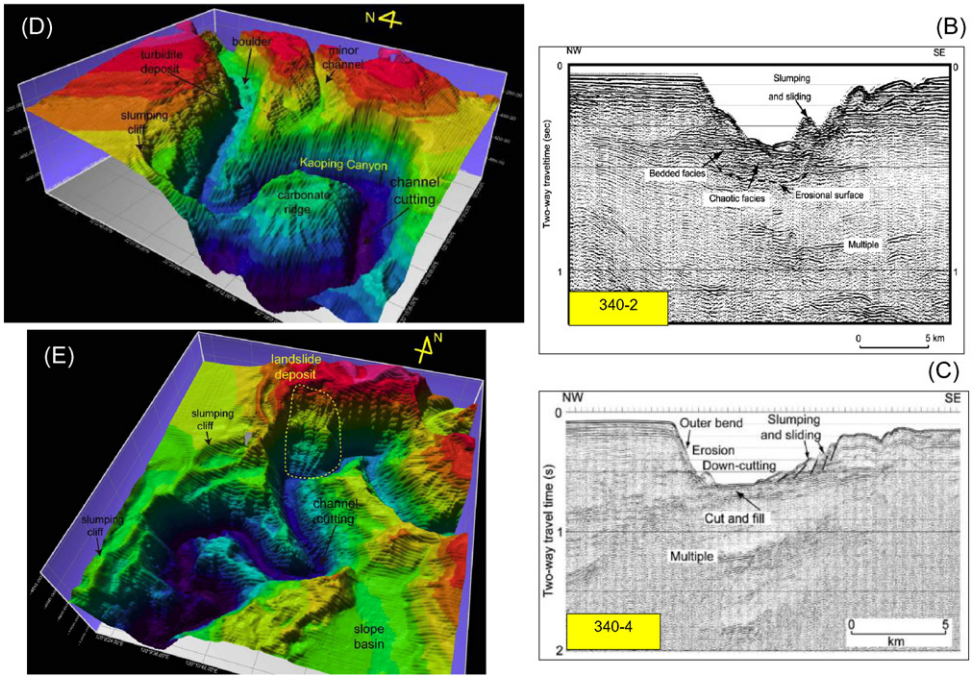

Fig. 6. (A) Detailed bathymetry of the upper reaches of the GPSC based on the composite of 3 multi-beam bathymetric surveys conducted by Taiwan Ocean Research Institute (TORI). The two black dashed lines indicate the locations of two seismic cross-sections (B, C). Localized canyon-rim slumping (D) and canyon-wall landslide (E) are indicated by red arrows on two 3-D topographic plots. (B is taken from Chiang and Yu, 2011; C is taken from Chiang and Yu, 2006; D and E are taken from Yeh et al., 2013).

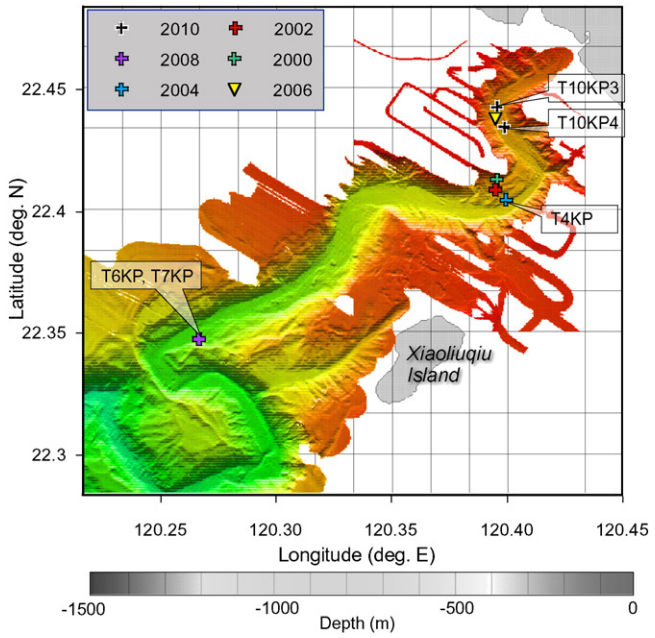

Fig. 7. The deployment locations of 6 taut-line sediment trap moorings and one shipboard hydrographic profiling station in different years (Liu et al., 2013) are plotted over the bathymetric map shown in Fig. 6.

water (Liu et al., 2002, 2006). The canyon interior is stratified mainly due to the temperature gradient (Liu et al., 2002), and slopes of isopycnal surfaces in the canyon are controlled by the tidal phase (Liu et al., 2002).

Tidal currents generally dominate the flow field in many submarine canyons, and internal tides may be an order of magnitude more energetic than the barotropic tidal currents (Kunze et al., 2002). Observations of currents and hydrographic profiles in the GPSC (Wang et al., 2008) show that in the lower part of the water column the major axis of the tidal currents is aligned with the thalweg of the canyon (Liu et al., 2010). Tidal energy is channeled from the shelf landward with a beamlike internal wave, guided by bottom topography. The semidiurnal internal tide (M_2) dominates with an intensity increasing with depth (bottom trapped) and is also increasing toward the canyon head (Wang et al., 2008). The water mass displacement associated with the internal tidal current may have had a major effect on the sediment transport (Xu et al., 2002; Liu et al., 2012). The internal tide can be easily generated and amplified with the isotherm displacement over 200 m and thus plays an important role in mixing, leading to downward mixing of river discharged materials over a tidal cycle. Note, the internal tidal energy flux in the GPSC is 3–7 times greater than that in the Monterey Canyon (Lee et al., 2009a,b). The isopycnal disturbances and associated high suspended-sediment concentrations near the canyon floor suggests that turbulent mixing and breaking of internal tides play a role in sediment transport processes in the canyon (Lee et al., 2009b; Liu et al., 2002).

In 2008, two sediment trap moorings were deployed in deeper water (~650 m) than previous deployments in the GPSC (Fig. 7): 1) January–March (T6KP) and 2) July–September (T7KP) (Figs. 1, 7). The observations from these two moorings reveal two fundamental patterns of the flow field and the associated sediment dynamics in the GPSC (Huh et al., 2009b; Liu et al., 2012). In each mooring dataset there is a clear demarcation between the shelf and canyon flow regimes (Fig. 8). On the shelf, the impinging flow of the Kuroshio Current and wind-generated currents dominate the sub-tidal flow field, and these are superimposed by tidal oscillations (Liu et al., 2006) (Fig. 8A, B). Under normal conditions the flow in the canyon interior shows a two-layered structure affected by the internal tide (Fig. 8A) (Liu et al., 2006, 2009c; Wang et al., 2008), which is better revealed by the measurements of an upward-looking long-range ADCP (Huh et al., 2009b). However, during the passing of four typhoons in the 2-month deployment of T7KP (Liu et al., 2012), the two-layer structure was replaced by a thick layer of landward flow almost filling the entire water column of the canyon interior, with a thin layer of seaward flow close to the canyon floor (Fig. 8B).

4.3.2. Benthic nepheloid layer

The benthic nepheloid layer has been observed in the head region of the GPSC throughout a year (Liu et al., 2002, 2010). The benthic nepheloid layer was as thick as 100 m and the suspended-sediment concentration reached 30 mg/l. The thickness and the suspended-sediment concentration of the benthic nepheloid layer are controlled by the tidal current in the course of a semi-diurnal tidal cycle (Liu et al., 2010).

Previous sediment trap moorings in 2000, 2002, and 2004 produced month-long time series records in the benthic nepheloid layer near the canyon floor of 1) along-canyon velocity, 2) water temperature, and 3) the volume concentration of suspended particles in various grain-size classes (Fig. 7). Data show that the benthic nepheloid layer is strongly modulated by the tides at semidiurnal, quarter, and sixth diurnal frequencies and spring-neap cycles (Liu and Lin, 2004; Liu et al., 2006, 2010). In

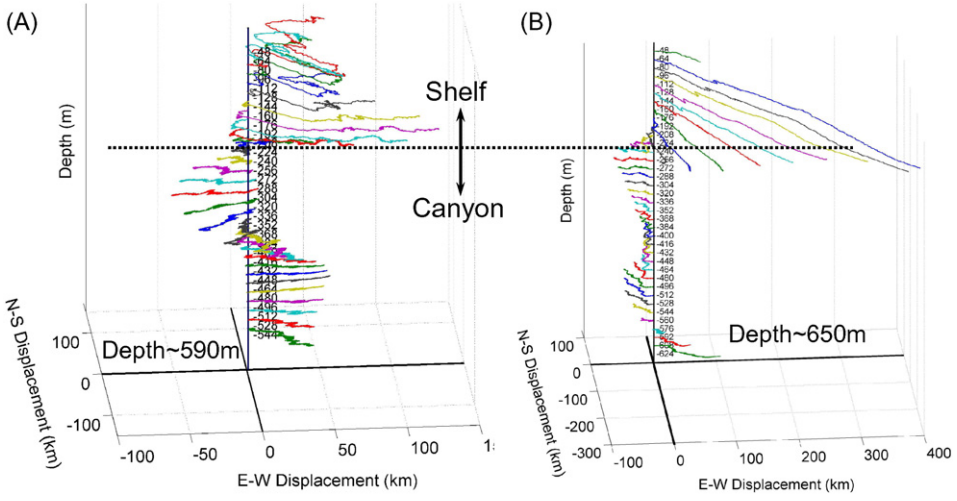

Fig. 8. Flow regimes above the canyon and in the canyon interior, differentiated as shown by the progressive vector plots of each bin in the ADCP measurements at the same location (Fig. 7) between 10 Jan. -20 March, 2008 (A) and 7 July–11 Sept., 2008 (B). (A) is taken from Huh et al. (2009b) and (B) is the re-plot of the data reported in Liu et al. (2012).

the course of a semidiurnal cycle, the flood (up-canyon) current brings colder and more saline offshore water containing higher suspended-sediment concentrations that enters the canyon near the canyon floor (Fig. 9A, B). This causes the thickness of the benthic nepheloid layer to increase. During the ebb phase, warmer and less saline coastal water displaces the colder and more saline water near the canyon floor. The suspended-sediment concentration immediately near the canyon floor increases in response to the maximum flood and ebb currents of the M_2

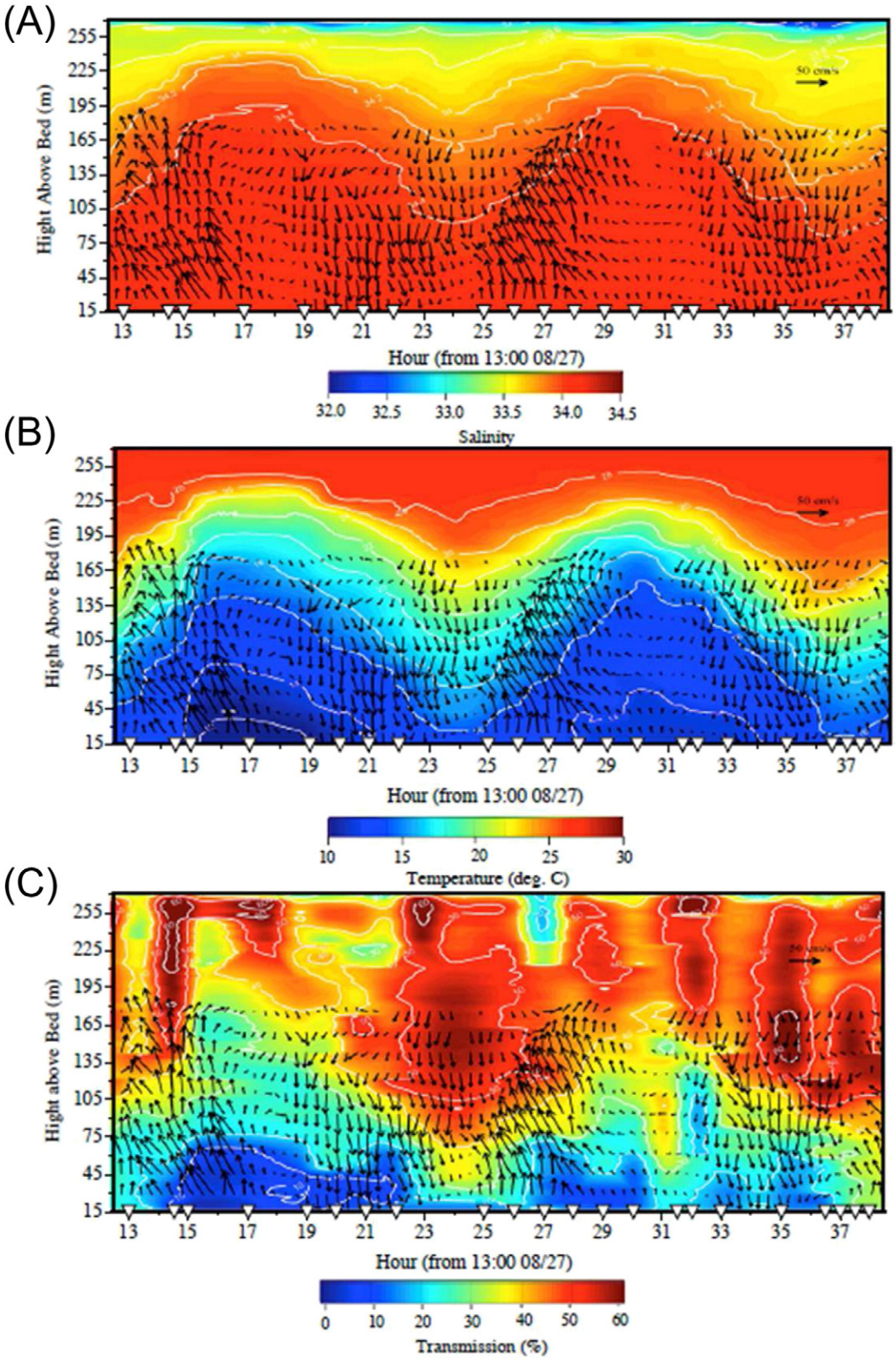

Fig. 9. Shipboard measurements of the tidally modulated benthic nepheloid layer as shown by the vertical changes over a 25-h period of (A) salinity, (B) temperature, and (C) light transmission. The simultaneously measured flow field is represented by the magnitude and horizontal orientations (north is to the top of the plot) of the arrows (taken from Liu et al., 2010).

tide (Fig. 9C). In the benthic nepheloid layer, suspended-sediment transport is also strongly affected by non-linear processes such as the generation of M_4 tide (the overtide of M_2), as indicated by the increased values of the amplitude ratios of M_4/M_2 for the suspended-sediment grain-size classes (Liu et al., 2010) and by the interaction between the internal tide and the canyon topography (Lee et al., 2009a).

4.3.3. Dynamics and sources of the settling particles

Liu and Lin (2004) show that river plume dynamics and the coastal wind field largely control the delivery of river and shelf-sourced terrigenous fine-grained sediment to the canyon under non-flood conditions. Based on theoretical settling velocities of siliciclastic spherical particles and assuming a still and stratified canyon interior, Liu and Lin (2004) found that sand-sized particles fall through the canyon within an hour while the clay-sized particles take over a month to settle. Consequently, the 'behavior' of suspended particles of different sizes in the canyon interior can be differentiated into a coarse-grained group (sand) that forms the 'rapid-settling' population and a fine-grained group (mud) that forms the 'background' population. The coarse-grained group is delivered directly to the canyon by the river effluent and by wave resuspension of the shelf substrate (Liu et al., 2012). Both lithogenic and non-lithogenic particles contribute to high mass fluxes including all sediment types (exceeding 700 and 800 g/m^2/d) in the lower part of the canyon (Liu and Lin, 2004; Liu et al., 2009c).

With lower settling velocities, fine-grained sediment remains in the water column longer and is transported farther, causing the observed downward fining of suspended-sediment in the canyon (Liu and Lin, 2004; Liu et al., 2009c). Because of the longer residence time of fine-grained sediment in the water column, there are also downward decreases of fine-grain affiliated non-lithogenic components in the suspended-sediment in the water column such as TOC and PAH due to decay, decomposition, and mineralization (Liu et al., 2009c).

4.3.4. Sedimentation: tide-dominated versus gravity-flow dominated regimes

Time-series data of water-borne properties and sediment captured by the sediment traps on T6KP and T7KP moorings provide clear insight into the dynamics of settling particles in the GPSC (Huh et al., 2009b; Liu et al., 2012, 2013). The two moorings had similar configurations, in which identical non-sequential sediment traps were used. They were also deployed near the same location, which makes them ideal to show contrast in the canyon hydrodynamics and sediment dynamics (see Sections 5.2, 5.3).

The T6KP mooring was deployed in the winter/dry season when tides were the dominant forcing in the GPSC. The spring-neap tidal cycles were well reflected in the textural composition and the mean grain size of the sediment captured by the sediment trap (Fig. 10A, F). The data show that higher energy during the spring tide caused increases in the coarse-grained faction (sand), which resulted in larger mean grain size (Fig. 10A). Conversely, the fine fraction was higher during the neap tide. Since the amount of clay controls the texture of the captured particles in the trap, the down-trap water content basically follows that of the clay content (Fig. 10B). These fine-grained particles are major carriers of bio-geochemical signals. For example, the TOC and TN mimics that of the clay fraction in the sediment trap samples (Fig. 10C, D). Liu et al. (2009c) also reported similar trends.

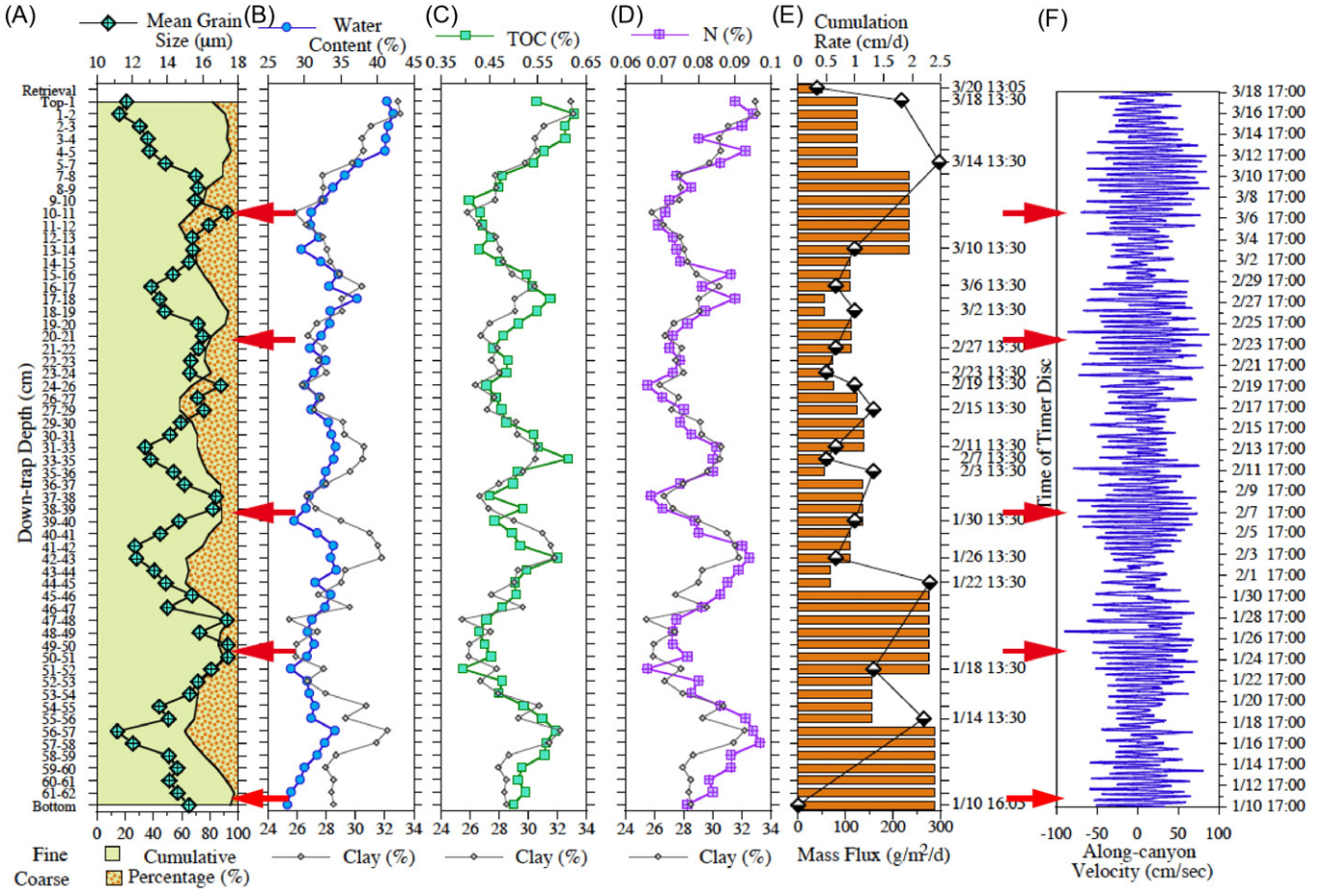

Fig. 10. Findings from the sediment trap mooring (T6KP) between January and March 2008 that show tidal-regime controlled dynamics of settling particles in the GPSC over 5 spring-neap cycles as revealed by the down-trap changes of (A) composition of the coarse and fine fractions and mean grain-size, (B) water content and clay fraction, (C) TOC and clay fraction, (D) TN and clay fraction, (E) cumulation rate (half-tone diamonds indicate the locations and time of timer discs) and mass flux (horizontal bars) between adjacent timer-discs, and the (F) corresponding along-canyon flow. The red arrows point to the time of the spring tide in the canyon.

The T6KP mooring encompassed five spring-neap cycles (Fig. 10F), which generally recorded an increase in the mass flux from a neap to the ensuing spring tide (Fig. 10E). Liu et al. (2009c) also documented the close co-varying relationship of the mass flux and coarser grain-size composition to the spring-neap cycle. During this deployment, most of the captured sediment was mud, of which the clay content was as high as 30% (Fig. 10B). This suggests the tidal regime provides a stable hydrodynamic environment for steady sedimentation of hemipelagic mud (Huh et al., 2009b), which is the normal sedimentation pattern in the GPSC. The sedimentation of mud leads to the dominant presence of mud on the seafloor of the GPSC (Liu et al., 2002, 2009c).

Being deployed in the summer/flood season, T7KP (Fig. 11A) experienced an energetic regime of hyperpycnal events followed by the quiescent normal tidal regime (Liu et al., 2012). This is clearly reflected in the grain-size texture and the mean grain size of the captured sediment (Fig. 11B). In the sediment trap sediment, Liu et al. (2012) identified sediment carried by two hyperpyncal turbidity current events, each characterized by an inverse graded layer overlain by a graded layer, then capped with a thin layer of fine-grained sediment (Fig. 11B). This is hypothesized to be the waxing and waning phases of the turbidity currents. However, the inverse-to-normal grading could also be caused by an increase in suspended-sediment concentration in the flow (Talling, 2014). The grain-size composition is much coarser during this period of typhoon influence. The normal tidally influenced pattern returns in the sediment in the upper part of the sediment trap (Fig. 11B). Three spring tides could be identified by the periodic pattern of higher sand content and a greater mean grain size shown by the captured particles (Fig. 11B).

Comparing the texture in the upper and lower part of the sediment trap (Fig. 11B), it is clear that sediments in the lower trap were coarser and had a higher settling velocity, pointing to a more energetic regime (Fig. 11C). The estimated mass flux during the 16-h period of the two hyperpycnal turbidity currents was 2 orders of magnitude higher than that measured during the spring tide (Liu et al., 2009c). This dataset suggests that the tide-dominated regime represents the hemipelagic background, in which the fine-grained sedimentation occurs. In contrast, the hyperpycnal turbidity currents triggered by the hyperpycnal plumes at the river mouth during episodic river floods appear to be the main agent (based on the mass flux) for coarse-grained sediment deposition and sediment transport in the canyon.

4.3.5. Tracers for terrestrial- and marine-sourced particles

Ubiquitous contaminants such as PAHs are mainly transported via atmospheric wet/dry deposition, air-water exchange and fluvial delivery in coastal areas. Nonetheless, they can also be transported through oceanic circulation and long-range atmospheric transport (Dachs et al., 1996; Fang et al., 2009, 2012; Huang et al., 2012; Lai et al., 2014; Lin et al., 2013; Sato et al., 2008). As these compounds are particle reactive, the specific patterns of their presence in particles can help trace particulate transport within a dispersal system (Fang et al., 2009; Huang et al., 2012; Lin et al., 2013). Several diagnostic ratios related to their provenance have been widely used to distinguish the possible sources of these particles (Fang et al., 2003, 2007, 2009; Huang et al.,

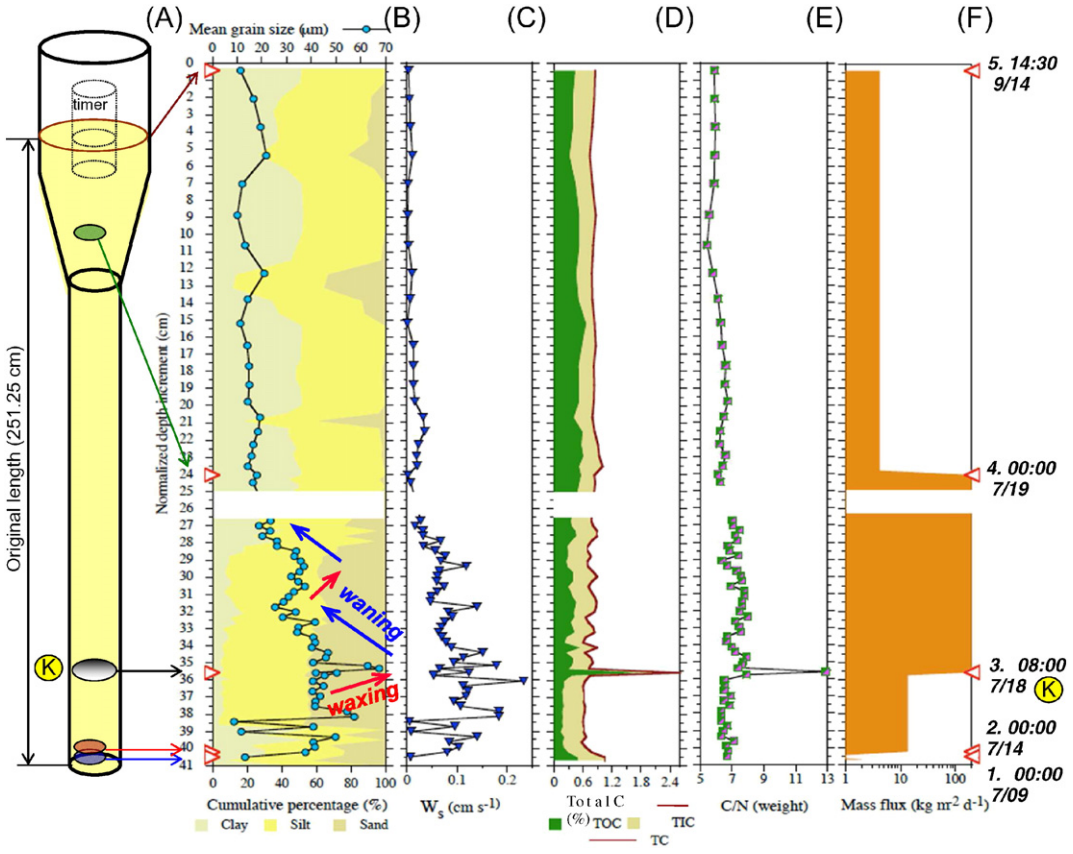

Fig. 11. Findings from the sediment trap mooring (T7KP) between July and September 2008 that show captured signals of two typhoon-triggered hyperpycnal turbidity current events. (A) Schematic drawing of the non-sequential sediment trap showing the level of collected sediment in yellow, physical locations of the 1st three timer-discs and their corresponding normalized down-trap depths (pointed by the arrows), and the location of the sediment 'interface' as indicated by the circled alphabet 'K' for Typhoon Kalmaegi. (B) The mean grain-size (blue circles) plotted over the cumulative percentage of clay, silt, and sand. The red and light purple arrows represent inferred waxing and waning stages of two hyperpycnal turbidity currents. (C) Settling velocity. (D) Total carbon (TotalC) as expressed by the summation of TOC and TIC. (E) C/N ratio by weight. (F) Mass flux. The right/left-hand pointing red triangles indicate the down-trap depths of the 5 time-points that delineate the intervals for estimating the mass fluxes. The blank segment indicates the space where the funnel of the trap is threaded into the PVC pipe below which the sediment sample was greatly disturbed in the disassembly process after retrieval (taken from Liu et al., 2012).

2011; Lai et al., 2011, 2013; Lin et al., 2013; Page et al., 1999; Savinov et al., 2000; Yunker et al., 2002). Three diagnostic ratios, representing petrogenic, biogenic and pyrogenic origins, have been effective in differentiating and characterizing sediments among offshore, nearshore and inner harbor samples in the Gaoping system, respectively (Fang et al., 2003). Enrichment of pyrogenic and petrogenic PAHs in sediments exhibit spatial dilution by biogenic PAHs, which can be used to infer their transport and origin.

Before PAHs were used as provenance tracers in southwest Taiwan, seasonal and spatial variations of PAH fingerprints in sediments were explored (Fang et al., 2007; Jiang et al., 2009). The sources of particulate PAHs in the water column of the GPR are predominantly petrogenic in the flood season but pyrogenic in the dry season. Samples used to characterize PAH compounds in the water column were collected from two taut-line sediment trap moorings (T4KP) deployed at the upper rim and near the floor of the canyon (Liu et al., 2006, 2010). PAH diagnostic ratios and statistical tools (e.g., principal component analysis) were applied to distinguish sources of PAHs and trace the transport path of the land-derived particles from the GPR (Fang et al., 2009). During the sampling period, both traps were significantly tilted by the tidal currents and fluctuated vertically (Lee and Liu, 2006; Liu et al., 2009b). The trap at the canyon rim experienced greater vertical movements, thus their particle characteristics (e.g., particulate organic carbon content, particle mass, and fine particle fraction) varied more than those from the trap near the canyon floor. Nonetheless, interesting observations were drawn from the study. Hourly depth variations of the tilted sediment trap array were echoed by the corresponding total PAH concentrations. The PAH composition of the collected particles was related to the flow direction and speed, reflecting alternating seaward (down-canyon) or landward (up-canyon) sources.

A second example illustrates the usefulness of PAHs to resolve the effects of a typhoon on particulate transport (Liu et al., 2012). Trap samples collected from T7KP provided a high resolution PAH profile that traced Typhoon Kalmaegi-induced particle movement (Liu et al., 2013). The PAH composition in the trap samples allowed the typhoon's effect to be broken into stages including; 1) marine signature before any typhoon; 2) signature of resuspended-sediments caused by typhoon-induced currents and waves; 3) pyrogenic particles from northwestern shelf caused by down-canyon flows; and 4) strong pyrogenic signatures caused by two hyperpycnal turbidity currents, suggesting the delivery of terrestrial particles. The anthropogenic PAHs discharged to the canyon head in the wake of the typhoon floods was indicated by low perylene ratios and these PAHs indicated a very clear petrogenic signal, representing the background composition of the GPR watershed.

In contrast to the PAHs, foraminiferal shells provide evidence for landward transport of biogenic particles of marine origin in the GPSC. During the distal phase of Typhoon Kai-tak (2000), the concentration of both benthic and planktonic foraminifera increased 2 to 4-fold in sediment trap samples (T1KP mooring) in the upper water column (104 mab, meter above the seafloor) and near the floor (54 mab) of the GPSC (Lin et al., 2005; Liu et al., 2006). The presence of shallow-water living benthic foraminiferal shells indicated landward transport in the canyon (Lin et al., 2005). The benthic and planktonic foraminiferal shells discovered in sediment traps on two moorings (T4KP) at the upper rim and near the floor of the canyon in 2004, also indicated lateral (cross-shelf) and up-canyon transport of biogenic marine particles (Liu et al., 2009b). These studies confirm that foraminiferal shells are not only useful tracers, but also important components of sinking particles in the GPSC (Liu et al., 2009b). Together, the tracers indicate two-way transport of particles in the GPSC.

5. The source-to-sink sediment processes in the GPR–GPSC system

In a conceptual model for the particle dynamics in the head region of the GPSC, Liu et al. (2009c) depict the diverse source and nature of particles, their complex delivery pathways to the canyon, and the sedimentation process in the canyon (Fig. 12). Generally, particles delivered to the canyon consist of three major types: 1) lithogenic/siliciclastic particles which are mostly sourced from the GPR and delivered by river plumes and from resuspension of shelf sediments; 2) biogenic

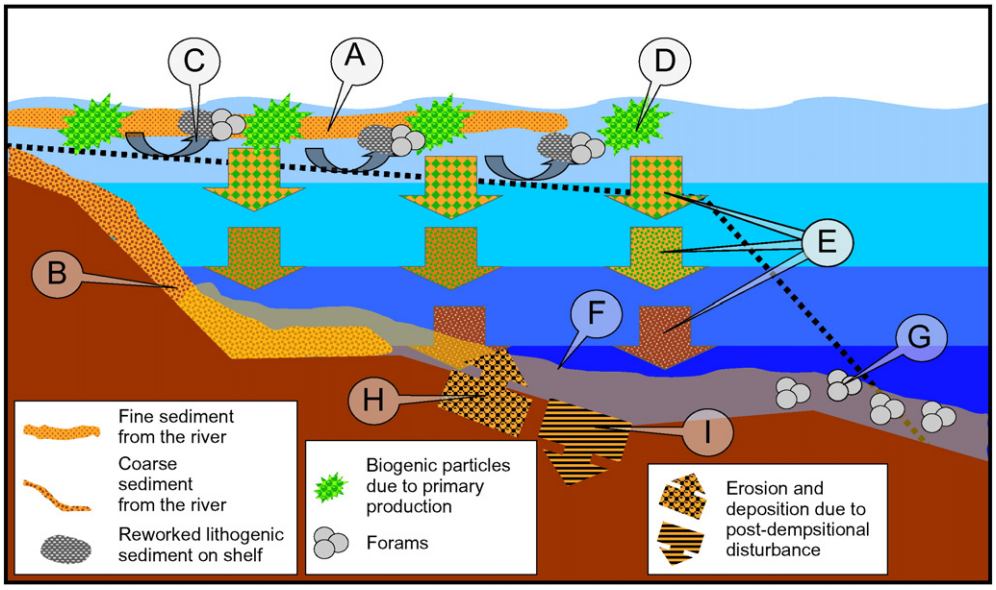

Fig. 12. A conceptual model illustrating particle dynamics in the head region of the GPSC. The thick dashed line depicts the upper and lateral boundaries of the canyon. The bands of different colors in the background indicate the stratified water column especially in the interior of the canyon. The legends in the first panel indicate particles from the fluvial and reworked shelf sources. The second panel represents particles of biogenic origins. The legends in the third panel include processes related to gravity-flow-caused erosion and deposition (hyperpycnites and turbidites). The meanings of the callouts are as follows: A: Fine-grained sediment is dispersed by the river plume on the shelf. B: Sediment coarser than very-fine silt descends into the canyon, a process that is modulated by the tide. C: Particles settling into the canyon are from diverse sources of terrestrial sediment, reworked sediment from the shelf floor, and biogenic particles related to marine foraminifers. D: Authigenic particles related to primary production on the shelf. E: Progressive change in physical and geochemical properties of sinking particles. F: Particles from resuspension from the canyon floor, entrainment from canyon walls, and along-canyon transport contribute to the formation of the benthic nepheloid layer. G: Planktonic and benthic foraminifers are significant biogenic particles transported from distal sources and from settling from above. H: Erosion of the substrate by gravity processes. I: Deposits by gravity flows such as turbidites and hyperpycnites. (Taken from Liu et al., 2009c).

particles related to primary production on the shelf, and planktonic and benthic foraminifera settling into the canyon from the shelf and/or transported up-canyon in its interior; and 3) reworked sediment due to failure of the canyon walls and entrainment from the canyon floor by gravity flows. Moreover, recent studies reveal that the river-sourced sediment, especially during floods, also contains terrestrial OC of multiple phases (Liu et al., 2012, 2013; Hsu et al., 2014; Sparkes et al., 2015). Transport agents including free settling, will be discussed in Sections 5.2 and 5.3. The estimated mass flux near the canyon floor is 2–7 times higher than that measured at the upper rim of the canyon (Liu et al., 2009c), suggesting that the extra sediment flux near the canyon floor could not have come from the upper water column in the canyon. Therefore, lateral transport along the canyon thalweg must be important in the lower part of the water column, probably within the benthic nepheloid layer of the canyon as has been documented in other canyon systems around the world (Arzola et al., 2008; Drexler et al., 2006; Puig et al., 2014; van Weering et al., 2002).

The physical and geochemical nature of particles is transformed as they settle through the water column in the canyon. Typically, there is a downward fining trend in the size composition of suspended particles as the average percentage of clay-to-fine-silt particles (0.4–10 μm) increases from 22.7% in the surface water in the canyon to 56.0% in the bottom water near the canyon floor. Conversely, the average percentage of the sand-sized (>63 μm) particles decreases with depth from 32% in surface water of the canyon to 12% in the bottom water near the canyon floor. As a result, the substrate of the canyon floor is composed largely of lithogenic hemipelagic mud. Along with this downward fining trend is the vertical decrease in the water column of the concentration of suspended non-lithogenic substances such as TOC and PAH, despite their affinity to fine-grained particles.

The downward change in the physical nature of the sinking particles is also reflected in the porosity and bulk (solids and voids) density of particles of three grain-size classes at the surface and near the bottom in the canyon. Hsu and Liu (2010) attribute this vertical variability to 1) flocculation, 2) biogenic processes, and 3) terrestrial-sourced sediment from the GPR effluent.

5.1. Fine-grained sediments as carriers of geochemical signals through the system

Fine-grained sediments are important vehicles for carrying geochemical signals along source-to-sink pathways of the GPS–GPSC system. An illustration comes from the combined studies of Liu et al. (2009a) and Hung et al. (2009) in which physical and geochemical properties of sediment on the riverbed of the GPR and the floor of the GPSC were investigated for the spatial variability along the river–canyon conduit (Fig. 13). The estuarine filter related to the salt-wedge creates a trap that retains higher levels of clay content on the riverbed that results in the elevation of all the measured geochemical variables of TOC, TN, Fe, Al, As, Hg, and Mn (Fig. 14, Liu et al., 2009a).

The spatial variability along the river–canyon pathway in the 8 geochemical variables was reanalyzed using the multivariate analysis technique of EOF (Empirical Orthogonal/Eigen Function) analysis. The results show that the first eigenmode explains over 52% of the overall correlation (standardized variance), indicating a high correlation. The sign of the eigenvectors of the first mode of all the variables is the same, meaning they all co-vary coherently (Fig. 15A). Clay particles are widely known as an efficient carrier for most particle-reactive trace metals and organics. Consequently, the eigenweighting curve of the first mode, which shows the spatial pattern of the mode, almost mimics the distribution of the clay content (Fig. 15B). This means that the distributions of the 8 geochemical variables are primarily controlled by the abundance of the clay (Fig. 15A).

The second mode explains over 24% of the correlation. In this mode, As, Al, Fe, and Mn co-vary with clay because Fe–Mn oxides/hydroxides are often coated on, or associated with, clay particles, leading to good correlations among them (Fig. 15A) This suggests that the Fe–Mn oxides/hydroxides are important in carrying metals, particularly for As (Hung et al., 2009). On the other hand, the organics and Hg co-vary in an opposite fashion to clay since Hg is abundant in the organic/sulfide fraction (Hung et al., 2009). Those sediments enriched in sulfide are likely derived from relatively reduced conditions with OM as a driver. Therefore, the eigenweightings of this mode become negative in the

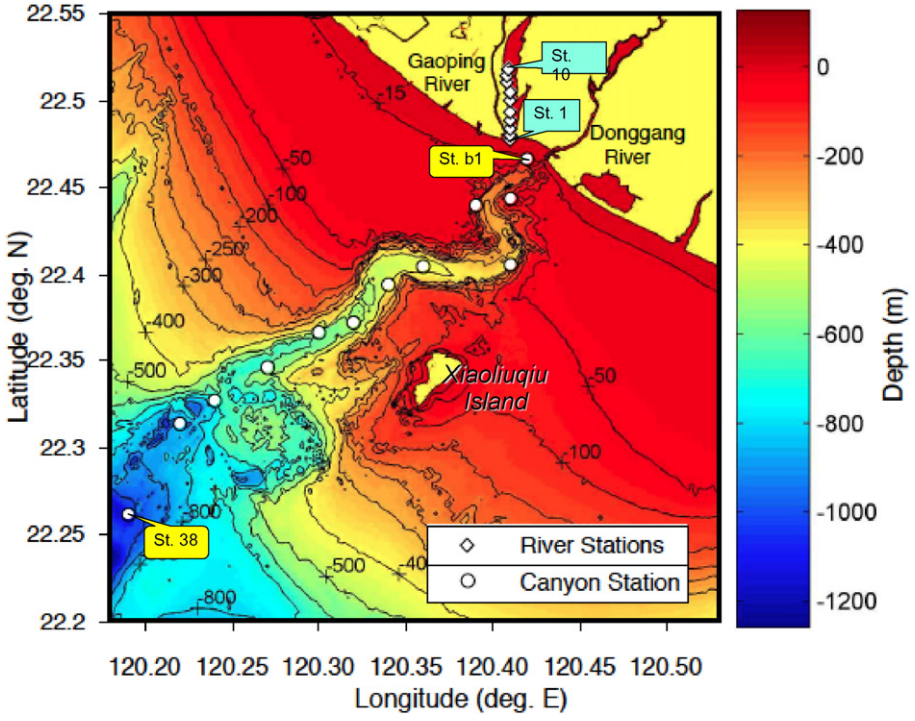

Fig. 13. Sampling stations from the lower reaches of the GPR to the upper reaches of the GPSC for a study of the geochemical control of organics and trace metals in the surficial sediment in the GPR–GPSC system in 2003 and 2004 (after Hung et al., 2009).

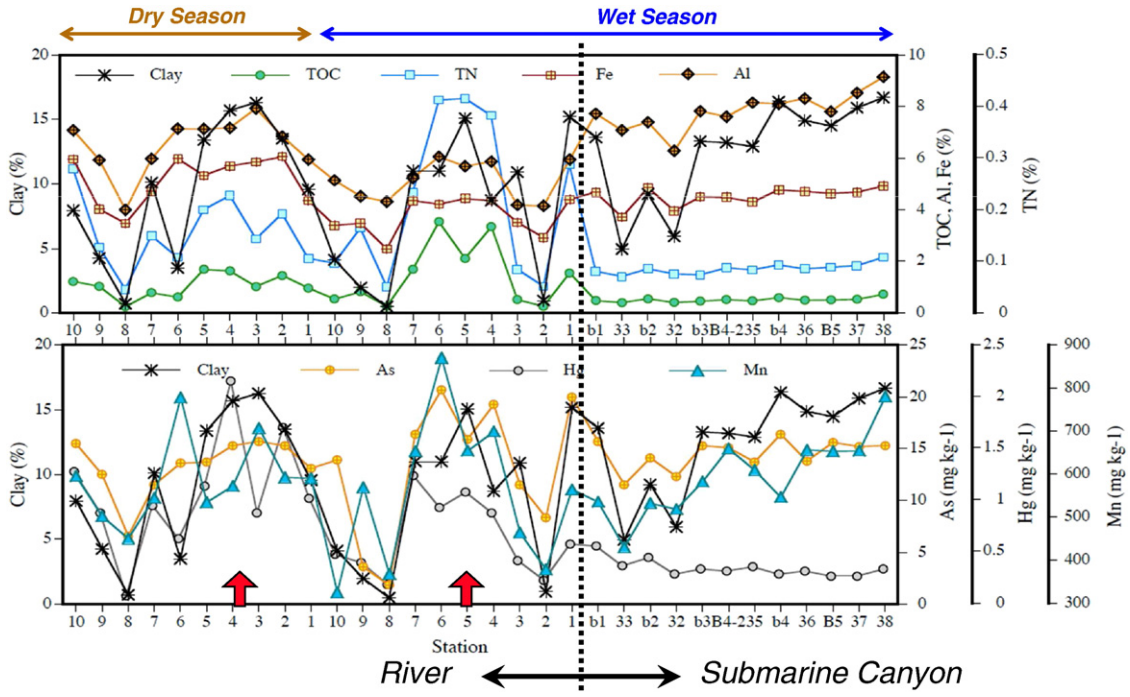

Fig. 14. The surficial sediment dataset of Hung et al. (2009) re-plotted to show the distributions of clay, TOC, TN, Fe, Al, (upper panel) As, Hg, and Mn (lower panel) along the river–canyon conduit. Stations designated by numbers were located in the river, the smaller the number, the closer to the river mouth. The along-canyon stations are designated by alpha-numerals, from b1 (at the head of the canyon) to 38. The two red arrows point to the locales of the estuarine filter (Fig. 5B) in both dry and wet seasons. The dashed black line separates the river and canyon regimes.

submarine canyon region (Fig. 15B), which is caused by the decomposition, mineralization, and degradation of the OM in the GPSC (Liu et al., 2009b; Hung et al., 2009). In summary, fine-grained particles (finer than medium silt) are the primary control of geochemical signals not only in suspended (Fig. 4) and settling (Fig. 10) sediments, but also in the substrate (Fig. 14) throughout the river–canyon system.

5.2. The river–canyon transport pathway under normal conditions

The two-month deployments of T6KP and T7KP provide valuable contrasts in the net sediment transport in the near-bottom part of the GPSC under normal and hyperpycnal conditions. The T6KP dataset only shows net displacement of water; suspended sediment transport

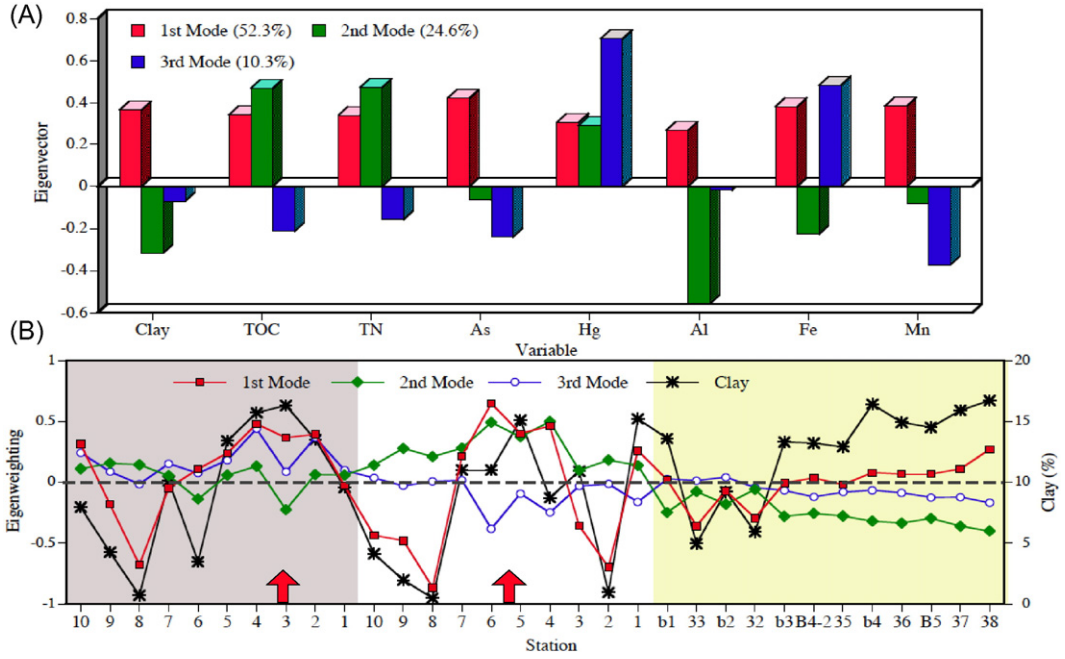

Fig. 15. EOF analysis results of the co-variability in the river-to-canyon geochemical properties of the sediment samples showing (A) groupings of the first three eigenmodes according to the sign of the eigenvector of each mode, and (B) the spatial characteristics of each mode according to the eigenweightings. The red arrows point to the locales of the estuarine filters in both seasons. The percentage of clay in each sample is plotted to illustrate the effect of gain-size.

should theoretically show an identical pattern (Fig. 16A). During the deployment in the non-typhoon season, the net water displacement was up-canyon, superimposed by tidal oscillations, both of which followed the orientation of the canyon axis at the mooring site (Figs. 7, 16A). This net transport pattern is mainly controlled by the tidal regime.

5.3. The river–canyon transport pathway under hyperpycnal conditions

The T7KP mooring revealed that the normal up-canyon directed tidal regime was interrupted by a typhoon-triggered down-canyon hyperpycnal regime (18–25 July), followed by a transitional period of recovery (25 July–24 Aug.). Eventually, the normal up-canyon tidal regime resumed (Fig. 16B; Liu et al., 2012, 2013).

Liu et al. (2012) provide the most comprehensive observations of not only the flow field of two passing hyperpycnal turbidity currents in the GPSC, but also the warm water and the terrestrial sediment that originated from Typhoon Kalmaegi-triggered floods in the GPR (Fig. 17). The estimated mass flux of these two sequential events in 16 h was 198.2 kg/m^2/d. The results further allow for an estimation of the sediment carried by the two hyperpycnal turbidity currents of 2.59×10^6 t.

Using discharge and suspended-sediment content from the Water Resources Agency, Ministry of Economic Affair, the sediment load in 2008 was 35.13×10^6 t, which is comparable previous studies (Dadson et al., 2003; Hung et al., 2012; Liu et al., 2008). Based on the average concentration of 0.58% for POC in GPR sediment (Kao et al., 2006), the average OC exported by the GPR in 2008 was roughly 24.4×10^4 t, comparable to that estimated by Hung et al. (2012). Using measured TOC (0.44%) and total carbon (0.83%) in the sediment carried by the two hyperpycnal turbidity currents (Liu et al., 2012), their total amounts are estimated, respectively (Table 1). The two hyperpycnal turbidity currents carried about 18% and 13.7% of the suspended-sediment and OC load exported by the GPR floods on July 18, 2008, respectively (Table 1). However, these low percentages are not surprising because the sediment trap mooring only captured the upper two thirds of the passing turbidity currents (Liu et al., 2012). Considering that the higher suspended-sediment concentration in the lower part of the turbidity currents was missing in the observation, the sediment load is likely underestimated. Further studies are needed on sediment gravity flows with improved observational tools.

After the passing of Typhoon Fanapi in 2010, Hsu et al. (2014) captured the wake of hyperpycnal turbidity currents in the GPSC using two taut-line moorings (T10KP3, 4; Fig. 7). Mooring T10KP4 was configured with a non-sequential sediment trap similar to that used by Liu et al. (2012). Although Hsu et al. (2014) missed the beginning of the hyperpycnal events, they did capture the warm water and the sediment carried by the hyperpyncal flow (Fig. 18). Their data showed a decreasing mass flux from 56.8 kg/m^2/d at the beginning to 1.24 kg/m^2/d at the end of the deployment over 5 days and 13 h. Although the hyperpycnal turbidity currents in the canyon were triggered under the same peak value of 20 kg/m^3 for the suspended-sediment concentration in the GPR during Typhoons Kalmaegi and Fanapi, the mass fluxes in the hyperpycnal turbidity currents after Typhoon Fanapi were much lower than during Kalmagei. This is probably because the Kalmaegi observation included two entire hyperpycnal events (Liu et al., 2012) whereas the Fanapi observation (Hsu et al., 2014) only included the wake of the hyperpycnal events.

In the Fanapi case, the average TOC in the sediment carried by the hyperpycnal flows was 0.44%, of which 70–90% was of terrestrial origin (Hsu et al., 2014). During Typhoon Kai-tak (in 2000) the TOC contents in captured sediment trap samples at the upper rim and near the floor of the GPSC were also about 0.4%, which is lower than 0.7% at the upper

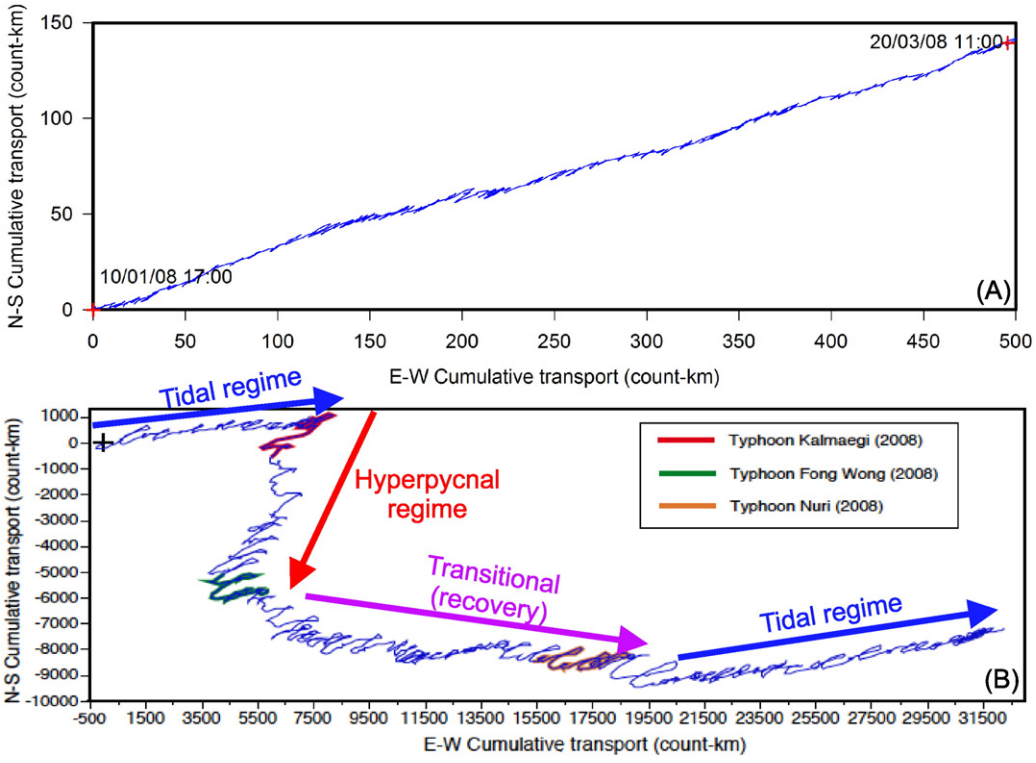

Fig. 16. (A) Progressive vector plot of the net water displacement measured at the sediment trap mooring (T6KP). The beginning and end time points of the record are marked. (B) Progressive vector plot of the net sediment transport observed at the sediment trap mooring (T7KP) (taken from Liu et al., 2013). The plot shows the normal tidal regime in the beginning of the record, which was then interrupted by the typhoon-induced hyperpycnal regime, followed by a transitional/recovery period, and at the end, the normal tidal regime returned.

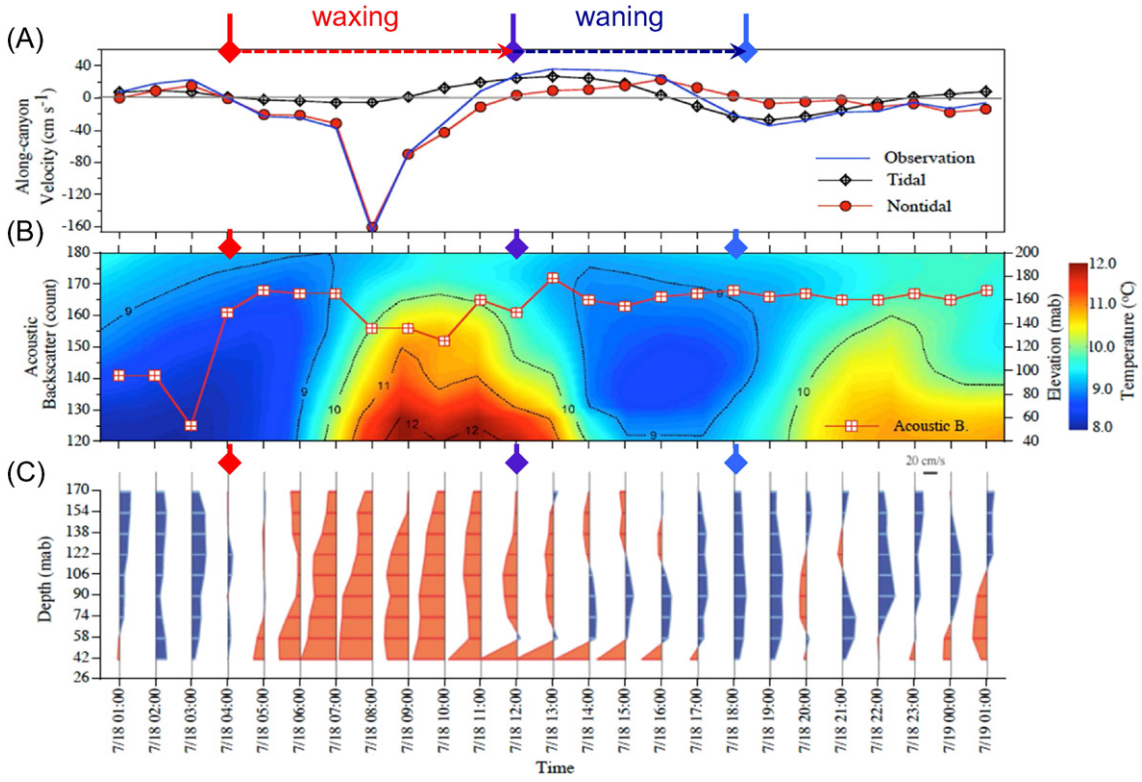

Fig. 17. Observations of two hyperpycnal turbidity currents in July 2008 by T7KP that include: (A) the tidal and non-tidal parts of the along-canyon velocity recorded by a single-level acoustic current meter at 56 mab (meter above bed); (B) contoured temperature and the acoustic backscatter measured on the mooring; (C) the vertical profile of the non-tidal along-canyon velocity measured by the RDI (LADCP) on a nearby mooring. The down-canyon flows are in red and up-canyon flows are in blue. The color-coded diamond time-markers indicate the beginning of the waxing phase (red), the transition from waxing to waning phases (purple), and the end of the waning phase (light blue) of the first turbidity current (taken from Liu et al., 2012).

rim and 0.5% near the seafloor for non-typhoon periods (Liu et al., 2006). Liu et al. (2006) attribute this decrease to a dilution effect caused by the increase of terrestrial lithogenic particles during the typhoon. However, this was not the case with the sediments carried in the head of a hyperpycnal turbidity current during Typhoon Kalmaegi (in 2008), when TOC content was as high as 1.92% (Liu et al., 2012). Since Typhoon Kalmaegi was the first typhoon in 2008, the initial river floods appear to have flushed out higher percentages of fresh organic matter (standing biomass) in the fluvial system, which was then carried by the hyperpycnal plume into the canyon and captured by the sediment trap. To summarize, both accounts of hyperpycnal turbidity currents in the GPSC confirm the river–canyon pathway for the delivery of terrestrial sediment and OC to the deep sea during typhoons.

In the GPSC, typhoon-related hyperpycnal turbidity currents originate in the fluvial environment, so the water they carry is warmer than the ambient water near the canyon floor (Kao et al., 2010). Consequently, from a temperature viewpoint, these flows are categorized as 'warm-water turbidity currents' (Fig. 19A-C). On the other hand, earthquakes (Talling et al., 2013) can also trigger mass failures, leading to the development of turbidity currents (Hsu et al., 2008; Carter et al., 2014). The water temperature of the turbidity currents of this nature should be the same or close to the ambient temperature of the canyon, forming 'cold-water turbidity currents' (Fig. 19D–F). In any case, either of these two mechanisms could generate gravity flows that have high speeds and long run-outs and are able to cause geohazards such as breaking subsea communication cables laid across the GPSC (Carter et al., 2012, 2014).

Since both warm- and cold-water turbidity currents are gravity-driven, the turbidites they deposit should have similar physical characteristics and typically consist of coarse-grained sediments with high amounts of lithogenic components (Liu et al., 2009c). A study has shown that turbidites deposited from warm-water turbidity currents

Table 1
Comparison of sediment and carbon loads and percentages of the two hyperpycnal turbidity currents and the GPR in 2008 (Liu et al., 2012).

Category	Sediment Load × 10^6 (t)	Total Carbon Load × 10^4 (t)	Organic Carbon Load × 10^4 (t)
GPR in 2008 (Liu et al., 2012)	35.13	–	24.4
GPR in 2007 (Hung et al., 2012)	37.0	35.1	22.6
GPR on July 18, 2008	14.40	–	8.35 (0.58% TOC content, based on Kao et al., 2006)
	41.0% of 2008	–	34.2% of GPR in 2008
Turbidity currents between 08:00–24:00 July 18, 2008	2.59	2.15	1.14
	18.0% of GPR on July 18	–	13.7% of GPR on July 18
	7.4% of GPR in 2008	6.1% of GPR in 2007*	4.5% of GPR in 2008

Note: All percentages are based on the river loads in 2008.

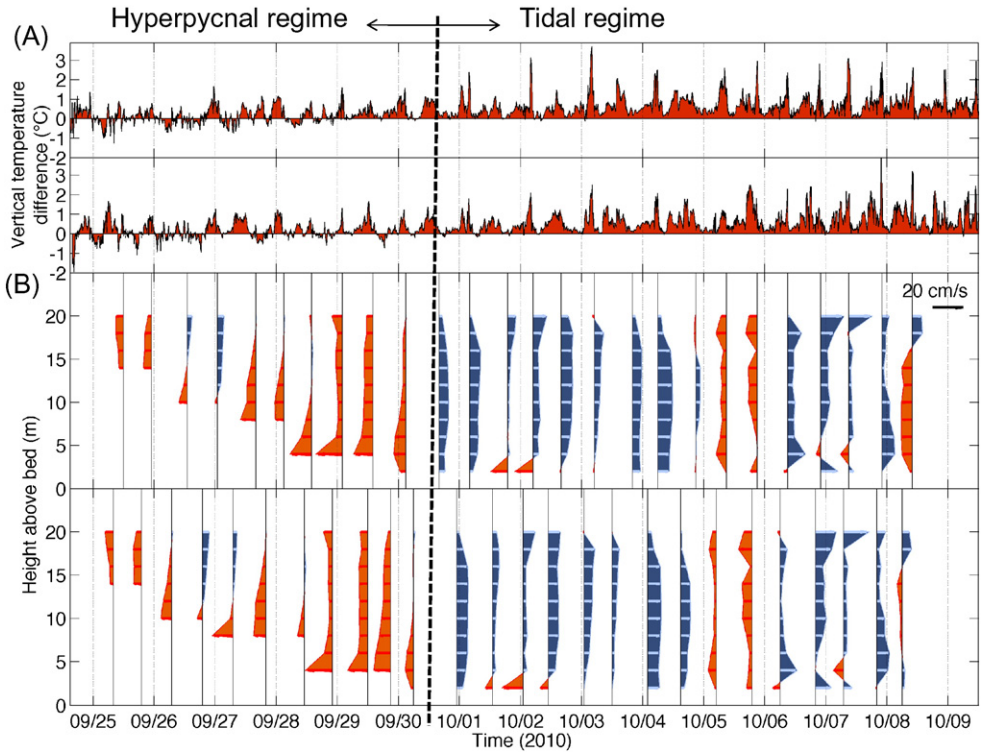

Fig. 18. Evidence of a river-flood related hyperpycnal event in the GPSC as shown by (A) the temperature reversals at the two moorings (T10KP3, 4), and (B) the vertical structure of the non-tidal flows observed at the two moorings. The positive and blue sticks indicate the up-canyon directed flows and the negative and red sticks indicate down-canyon directed flows. The black dashed line separates the hyperpyncal and tidal regimes of the flow field (taken from Hsu et al., 2014).

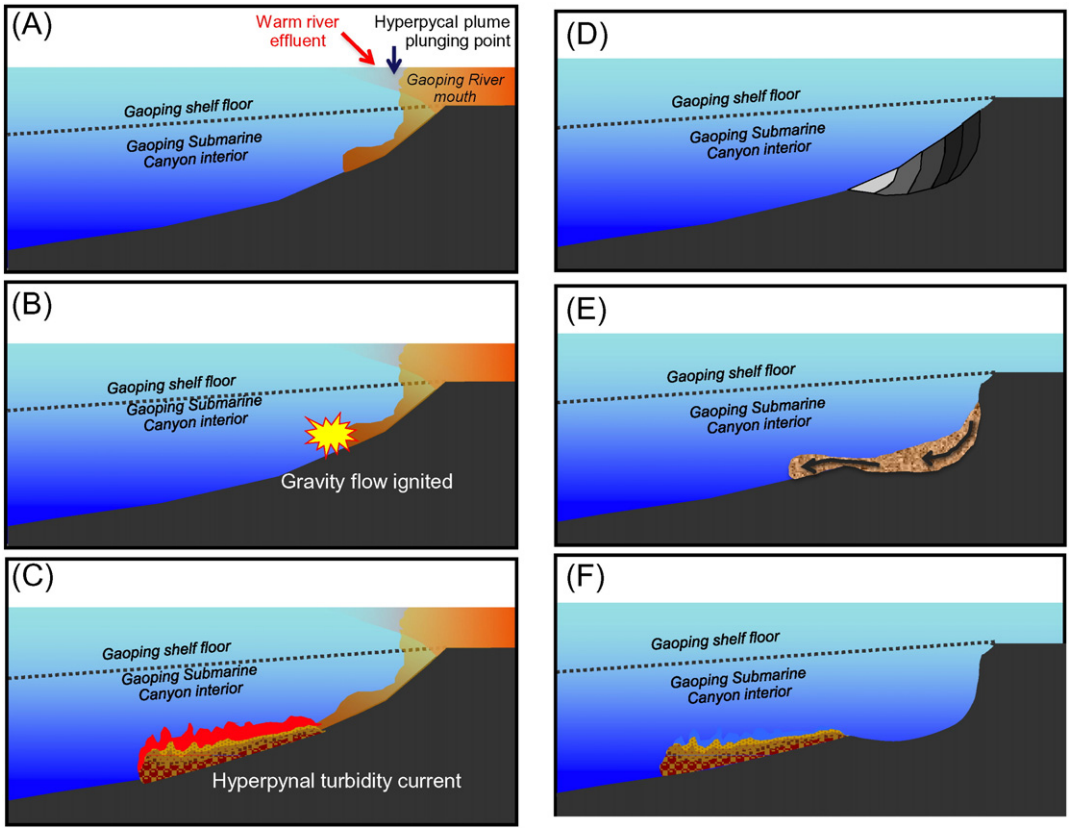

Fig. 19. Schematic drawings of the genesis of the 'warm' and 'cold' gravity flows in the GPSC. (A) During episodic flood events the GPR effluent containing high concentration of suspended-sediment forms the hyperpycnal plume and plunges into the head of the GPSC. (B) The hyperpycnal process ignites gravity flows. (C) Hyperpycnal turbidity currents carry warm water and a large amount fresh terrestrial sediment down the canyon. (D) Earthquakes or other marine processes cause the failure of canyon walls and slopes. (E) Slumping occurs and generates debris flows. (F) Through a hydraulic jump, the debris flows transform into turbidity currents carrying the ambient seawater and reworked marine sediment down the canyon (Talling et al., 2013).

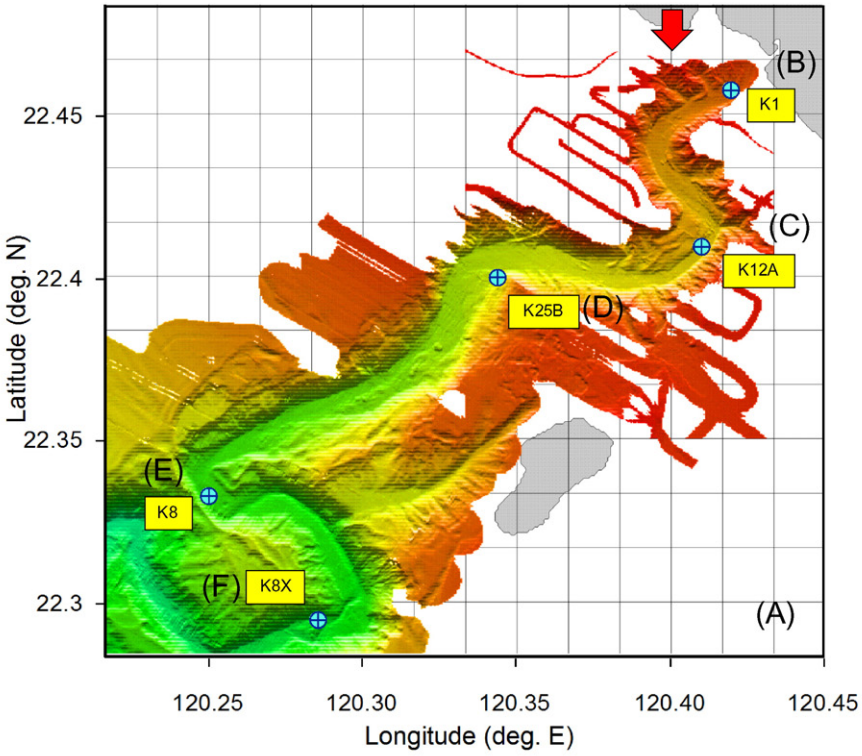

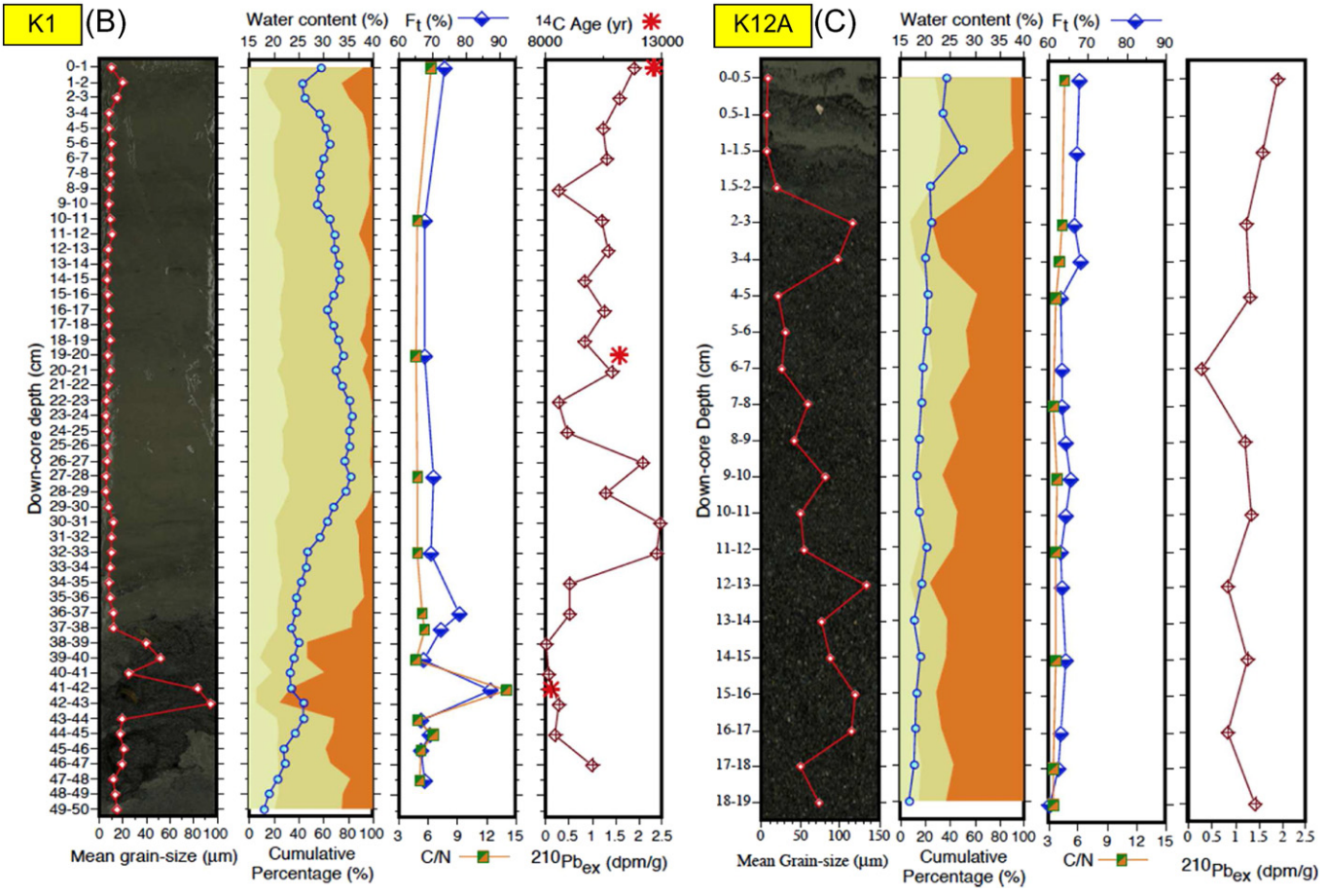

Fig. 20. (A) Map showings locations of 5 gravity cores along the thalweg of the upper reaches of the GPSC taken shortly after Typhoon Morakot. The core labels match the locations on the map (B, C, D, E, F). For each core, the following down-core variables are shown in sequence: the mean grain-size plotted over the photo of the core, cumulative plot of the sand, silt, and clay and water content, the Terrestrial Fraction (F_t) and the C/N ratio, and the $^{210}Pb_{ex}$. Core K1 has additional three data points of AMS ^{14}C age (provided by Robert Sparkes) plotted over the $^{210}Pb_{ex}$ curve.

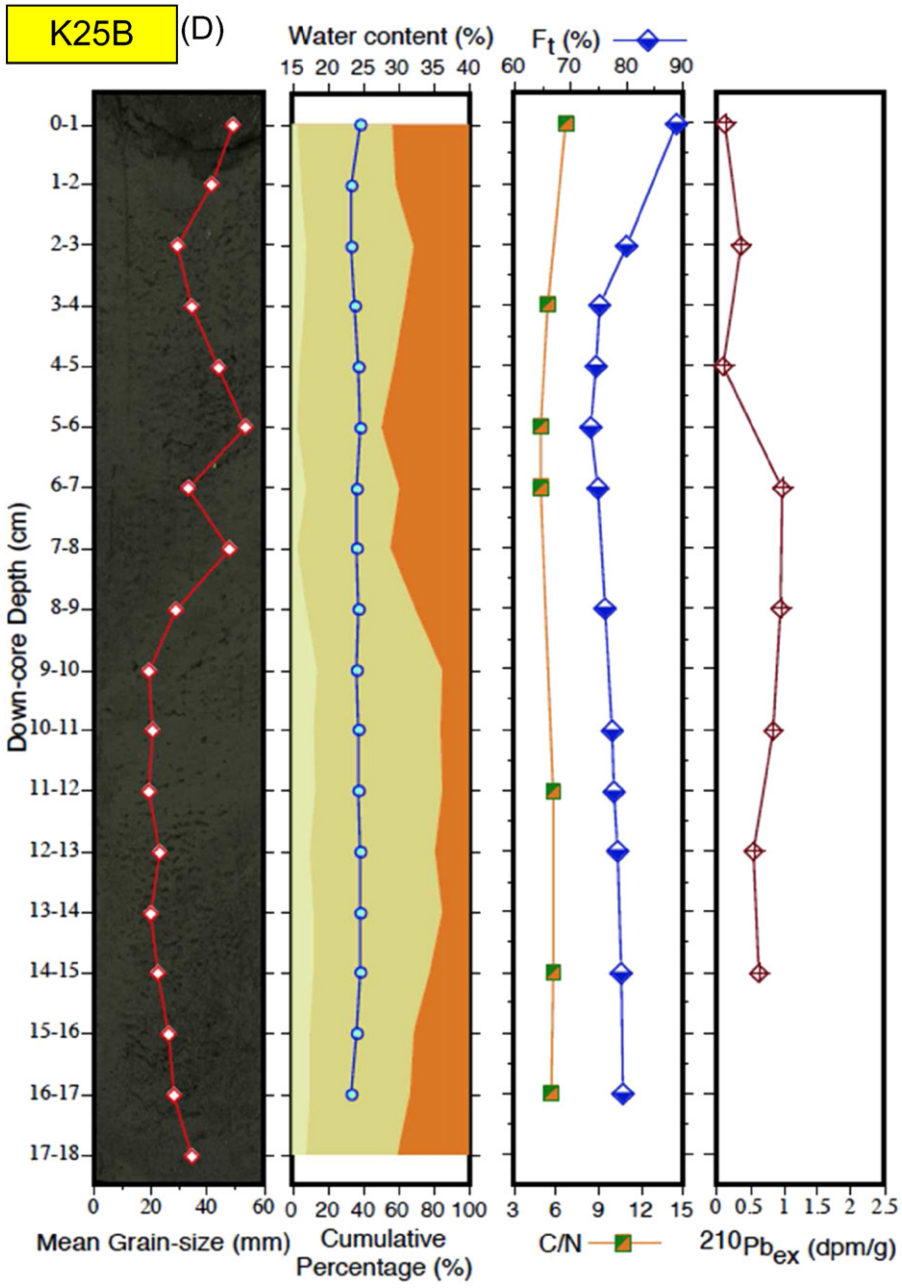

Fig. 20 *(continued)*

potentially contain fresher sediment from the terrestrial environment, having high values of terrestrial OC and water content and low to very low levels of $^{210}Pb_{ex}$ activity (Liu et al., 2009c). Conversely, turbidites deposited from cold-water turbidity currents are mainly reworked coarse marine sediment, having marine-sourced OC and low water content, and potentially very low levels of $^{210}Pb_{ex}$ activity (Liu et al., 2009c).

5.4. Internal sources and sinks: the new is old

The GPR–GPSC system is an active sediment dispersal system that links the mountainous river catchment to the deep sea via a submarine canyon. Typical sediment processes operate over tidal, sub-tidal to seasonal time scales. However, episodic typhoon and earthquake events dominate the system and move large amounts of sediment down the canyon and to the South China Sea (Carter et al., 2012).

Typhoon Morakot devastated the GPR catchment and left depositional layers not only in the GPSC but also in the nearby Fangliao Submarine Canyon (Hale et al., 2012). Several lines of evidence in five cores from the upper GPSC taken after this typhoon show flood-triggered hyperpycnal turbidites (Fig. 20). Notably in Core K1 located right at the head of the canyon, where plunging of the hyperpycnal plume probably took place, is a turbidite layer that contained over 80% of sand and high amounts of terrestrial OM (with TOC exceeding 1.0%), terrestrial fraction (F_t) exceeding 80%, a C/N ratio exceeding 14 (Liu et al., 2013; Sparkes, 2012; Sparkes et al., 2015), and very low $^{210}Pb_{ex}$ (Fig. 20B). Three AMS ^{14}C dated samples show the ages for the core material are 8.2, 11.2, 12.7 ka. (data provided by Robert Sparkes) in the turbidite, mid-core, and the core-top, respectively. The turbidite was likely fresh terrestrial sediment delivered by Morakot-related river floods, yet the OC it contained is over 8200 yr old. The ensuing deposited sediment

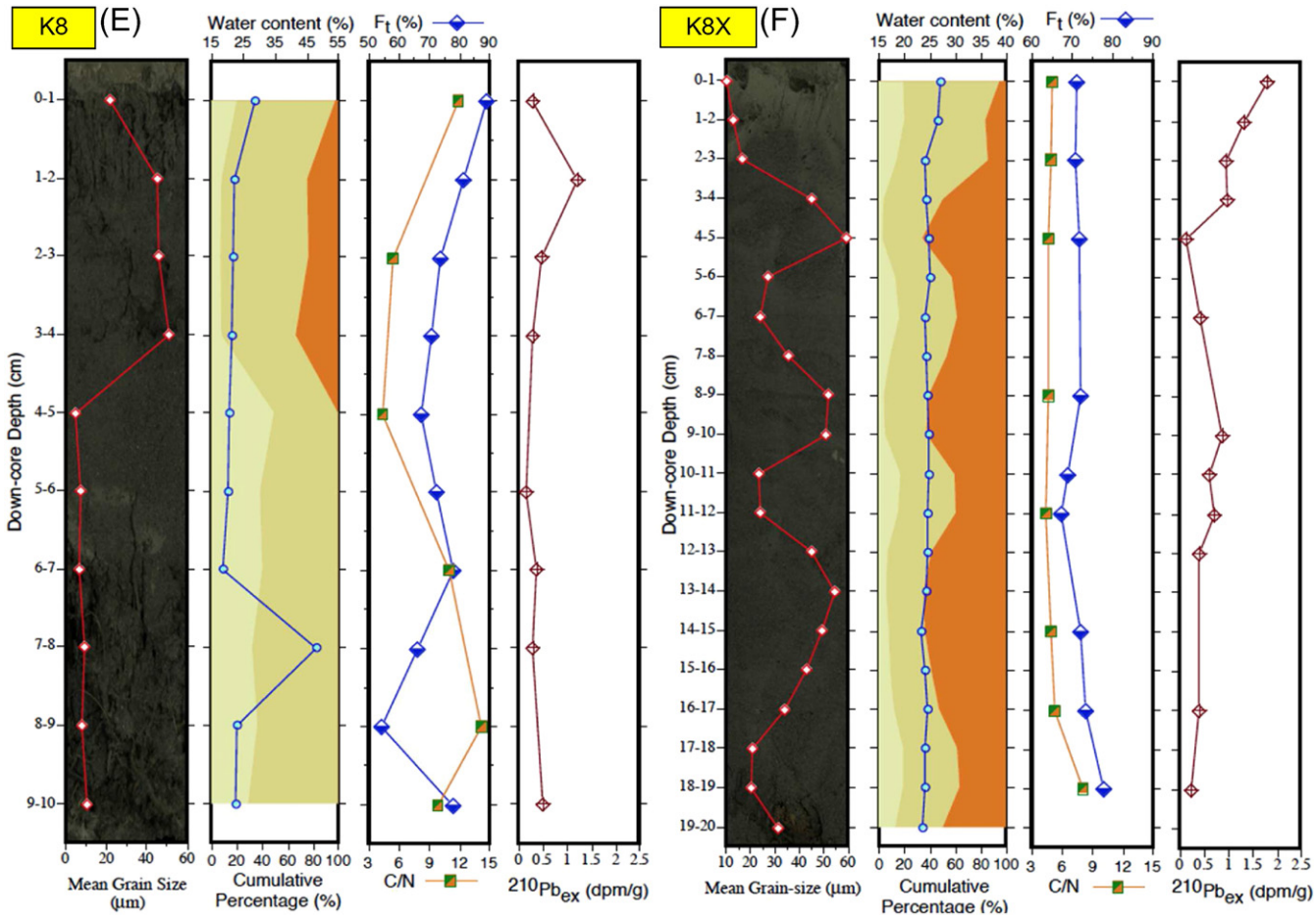

Fig. 20 *(continued)*

was medium silt, still containing over 70% of terrestrial OM, and is even older. Furthermore, the upward linear increase of $^{210}Pb_{ex}$ activity in the top 5 cm of the core probably reflects the scavenging effect due to steady sedimentation of terrestrial sediment after the floods. The old age of freshly delivered terrestrial sediment points to multiple sources for the sediment, particularly the OC from the terrestrial system (Hilton et al., 2011a; Sparkes et al., 2015). Typhoon-induced mass wasting and debris flows in the river catchment apparently 'released' the old sediment including fossil OC and mixed it with the fresh sediment that contained the terrestrial non-fossil carbon (Sparkes et al., 2015) during the transport process. This turbidite was probably deposited at the beginning of the river floods, with a higher amount of eroded topsoil, making it younger than the overlying sediment. As the typhoon progressed, older fan terraces, tributary fans, and ancient colluvium began to be incised, introducing older and finer sediment into the river flow which was then deposited in the wake of the peak floods forming the finer sediment deposited above the turbidite in K1 (Fig. 20). This phenomenon highlights the fact that fresh sediment newly delivered to the sea from highly disturbed river catchments contains old sediment with fossil OC (Sparkes, 2012) from internal sinks and deep erosions of the hill slopes, landslides, and fan terraces. This freshly delivered sediment that contains terrestrial fossil OC from the fluvial system is different from the reworked sediment from the seafloor found in sediment records that bears marine signals (including marine OC), which had already been delivered and deposited in the offshore part of the system (Kao et al., 2014).

Liu et al. (2002) found high abundance of very-coarse and coarse sand in the surficial sediment on the north flank of the canyon head. Recent multi-beam bathymetric surveys show gullies on the canyon wall at this location (pointed by the red arrow in Fig. 20A), which are likely erosional features from descending/plunging hyperpycnal plumes. The presence of the turbidite in Core K1 suggests that there might be another internal sink of temporarily deposited coarse-grained terrestrial sediment at the head of the canyon. These deposits may have been flushed down the canyon by the second flow described by Carter et al. (2012), or later by other hyperpycnal events (Puig et al., 2014).

After Typhoon Morakot, hyperpycnal turbidity currents may have been ignited at the canyon head multiple times and then moved down the canyon over a period of a few days (Kao et al., 2010; Carter et al., 2012). Due to topographically induced secondary flows and tidal energy distribution at the first meander of the canyon thalweg, erosion of the canyon floor and wall at the core site K12A is suspected to have caused the high percentage of sand at this site (Fig. 20C, Liu et al., 2010). Additionally, the lower F_t and C/N and high $^{210}Pb_{ex}$ values, suggest that the substrate sediment at this location is probably a mixture of marine and terrestrial material, including sediment from hemipelagic settling (Kao et al., 2014). After passing the first canyon meander, acceleration of the turbidity current due to the increased slope likely caused erosion at the location of Core K25B (Fig. 20D). In Cores K8 and K8X, turbidites are present showing higher values of F_t and C/N, and low $^{210}Pb_{ex}$ values (Fig. 20E, F). These two cores also contain coarse woody debris and the highest presence of terrestrial biomass of any of the Morakot cores (Sparkes, 2012; Sparkes et al., 2015). At the sites of Cores K8 and K8x, the canyon topography probably caused the turbidity current to decelerate (Fig. 20A), thus becoming depositional (Sequeiros et al., 2009).

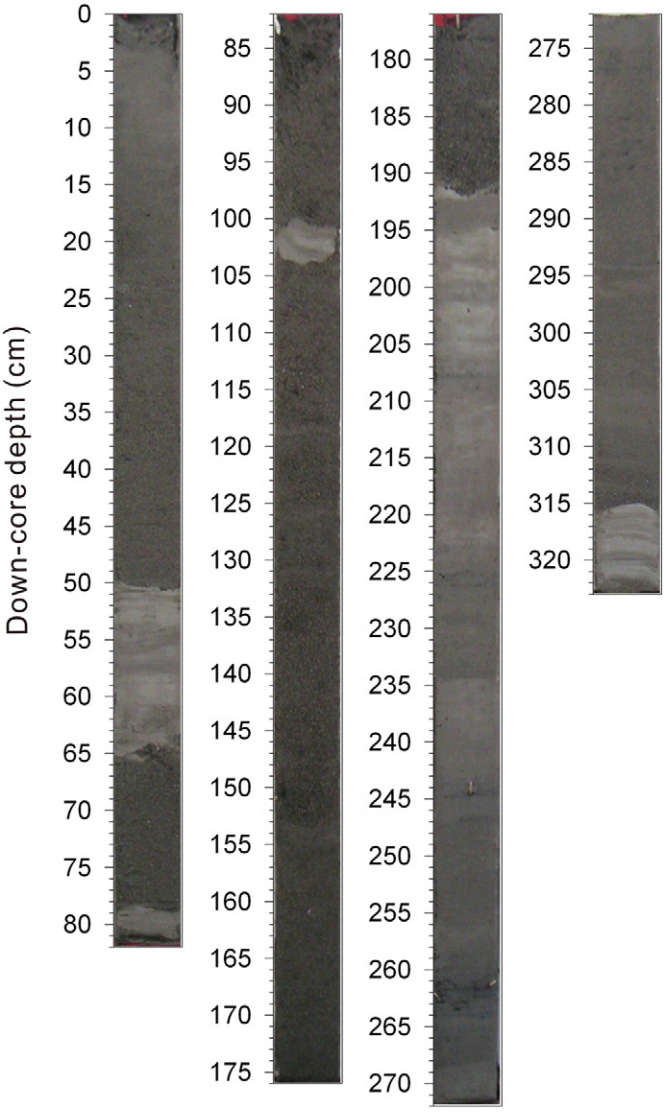

Fig. 21. Photo of Core OR1-811 K08P.

The low values of F_t, C/N, and $^{210}Pb_{ex}$ are also likely to have been contributed to by internal sinks from canyon wall slumping (Fig. 6B-E). Using elemental and isotopic analyses, Sparkes et al. (2015) confirmed that terrestrial OC (fossil and non-fossil) dominated the sediment in Morakot canyon cores. In the down-canyon transport by hyperpycnal turbidity currents, reworked marine sediment (resuspended from the shelf and from erosion of the canyon wall) including marine-sourced OC was also incorporated into the deposits (Sparkes et al., 2015).

Complementing the presence of fossil OC in terrestrial sediment freshly deposited in the Morakot cores, fossil OC contained in suspended terrestrial sediment was also captured in the non-sequential sediment trap immediately after Typhoon Fanapi (Hsu et al., 2014). The AMC ^{14}C ages of three sediment samples at the bottom, middle, and the top of the trap, were 7.8, 6.4, and 8.1 ka, respectively (data provided by George Burr), and corresponding F_t values were 82.2%, 92.2%, and 94.4%, respectively. Since sediment captured by the sediment trap was from the wake of hyperpycnal turbidity events (Hsu et al., 2014), the upward increase in the F_t values suggests that the weakened turbidity current reduced mixing with the ambient canyon water. This caused less dilution by marine-sourced OC in the captured terrestrial sediment, causing the upward increase in F_t values in the trap. There is no doubt that the typhoon-related events eroded modern OC and remobilized fossil OC in sediment from internal sinks in the GPR basin and transported them to the deep sea along the GPR–GPSC dispersal system via turbidity currents (Kao et al., 2014; Sparkes et al., 2015).

5.5. Sediment record signatures of the dual sedimentation pattern along the canyon conduit

Steady tidal oscillations and episodic sediment-gravity flows leave two distinct types of sedimentary signatures in seafloor deposits of the canyon conduit. Trends similar to those observed in the sediment trap moorings (Huh et al., 2009b and Liu et al., 2012) were also observed in longer piston cores taken at three locations: 1) proximal to the head in upper reaches (OR1-811 K08P), 2) at the transition between the upper and middle reaches (OR1-820 35), and 3) more distally, at the transition between the middle and lower reaches (OR1-811 K31A) of the GPSC (Fig. 1). They are used to illustrate gradual down-canyon changes in the seafloor lithology in response to the relative dominance of these two sediment transport processes.

Based on the core descriptions, the sediments at all three sites consist largely of fining-upward deposits, with coarser sandy units interspersed with bands of finer muddy units (the extent, depending on location within the GPSC). The coarser sandy-silt layers are dark greenish grey, while the finer clayey-silt layers are olive grey. Sporadic dark olive brown layers also occur. The coarser sandy units most likely reflect sediment-gravity flow deposits, while the finer muddy units represent hemipelagic deposits (Rendle-Buehring et al., 2009). The finer muddy units in the other two cores are dominated by sediments that are comparable to two pelagic, undisturbed long cores (ORI 799-G24 and ORI 732-8G) located outside the GPSC in the northeastern area of the South China Sea (Rendle-Buehring et al., 2008).

Core OR1-811 K08P is dominated by thick, very coarse, sandy turbidite deposits interspersed with minor thin bands of hemipelagic mud (Fig. 21). These findings suggest that this location along the canyon conduit forms a depocenter and a major sink for very coarse turbidite deposits left by turbidity currents generated farther up-canyon (Rendle-Buehring et al., 2009).

The lithology of Core OR1-820 35 consists mainly of clayey-silt intermingled with thin bands of coarser (sandy-silt) turbidite deposits (Fig. 22A, B). Many of these turbidites have the typically sharp lower boundary defined by a contrast in color, texture and grain size when compared to the hemipelagic background mud below (Fig. 22C). Graded laminations in the turbidites are also apparent in the X-radiograph (Fig. 22B). The fine-grained nature of the coarser deposits suggest that only the finer sediments carried in turbidity currents reach this location far down the conduit.

At the most distal Core OR1-811 K31A, the lithology is again dominated by fine-grained silty-clay and hemipelagic sediments. Interspersed in the hemigelagic sediments are minor intermittent fine-grained (<100 μm) thin turbidites (Fig. 23A). Due to the very fine-grained nature of these turbidites, they are more visible in the X-radiographs (Fig. 23B). The results suggest that only the very low energy (end) phase of the turbidity currents deposit sediment this far down the GPSC.

The sedimentary lithology observed in these three cores shows that grain size decreases down-canyon in both the fine-grained hemipelagic sediments and in the coarse-grained gravity flow deposits. This demonstrates the down-canyon decrease in the strength of the fluvial-fed sediment load and/or the episodic sediment-gravity flows (Talling et al., 2013). These results probably indicate that the upper reaches of the GPSC constitute a sink for the high-energy, coarser turbidites, while the middle and lower reaches of the canyon form a sink for the progressively lower-energy, thinner and finer-grained turbidites that are deposited in the more distal reaches of the canyon conduit. Farther away from the head of the canyon, the fine-grained mud becomes

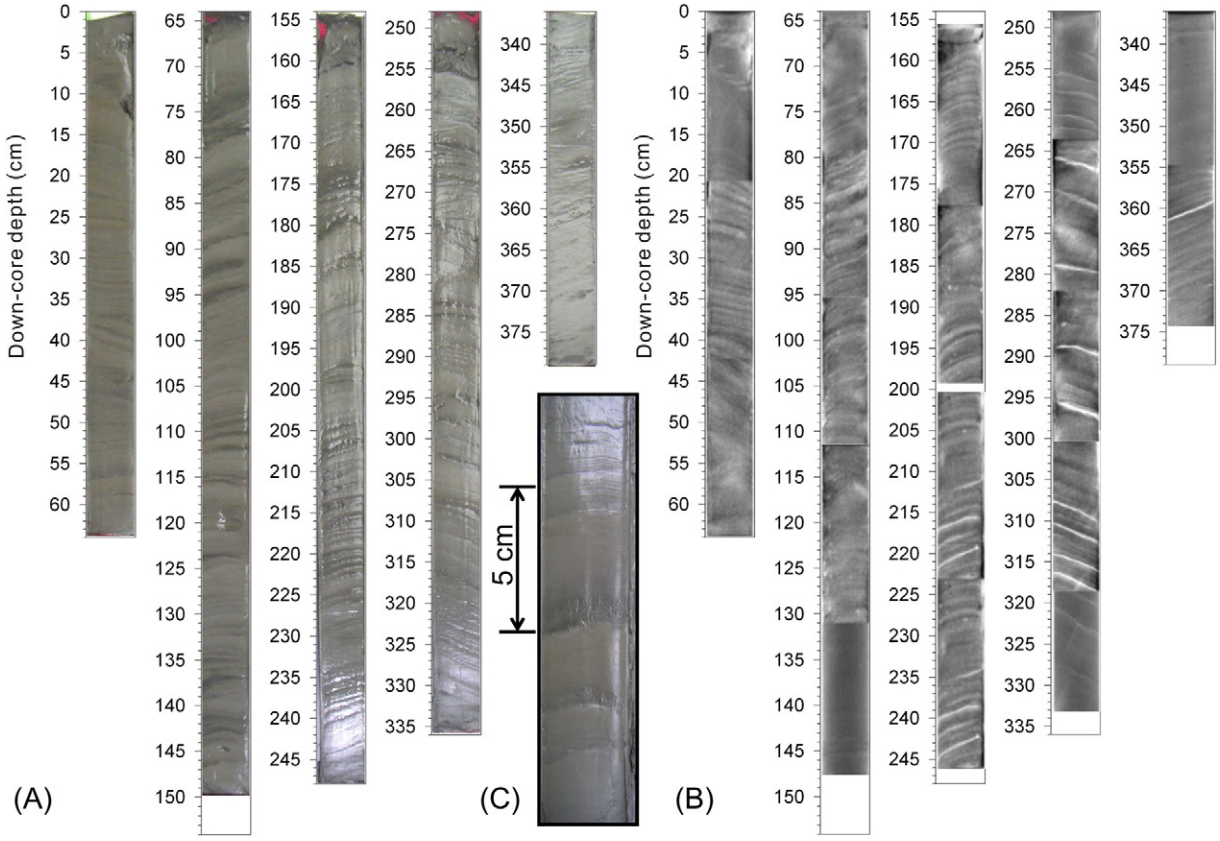

Fig. 22. Photo of Core OR1-820 35 (A), images of the X-ray radiograph of the segments of the core (B), and an enlarged photo showing a turbidite layer and the hemipelagic mud above and beneath it (C).

the dominant lithology in the more distal gravity flow deposits. These fine-grained mud deposits in the canyon are comparable to the hemipelagic sediments on the Gaoping slope (Sparkes et al., 2015) that ultimately form the deposits on the abyssal plain and in the Manila Trench in the South China Sea (the ultimate sink for sediments).

6. Summary and future work

The GPR–GPSC dispersal system is an interesting natural laboratory because it consists of a high-yield river basin that is dynamic in its sedimentary behavior and a submarine canyon whose sediment dynamics are controlled by tidal oscillations under normal conditions and by gravity flows under typhoon-induced hyperpycnal conditions or triggered by earthquakes. A river–canyon pathway is formed by complex mechanisms to deliver sediment of terrestrial, marine, and biogenic material with diverse physical and geochemical properties into the canyon. The submarine canyon is a two-way conduit facilitating land-sea interactions. Under normal tidal influence, the net sediment transport direction is up-canyon. Under episodic typhoon conditions, the net sediment transport is down-canyon by energetic gravity flows that deliver terrestrial sediment and carbon to the deep sea. There are two modes of sedimentation pattern in the canyon. The hemipelagic mud is formed in the tidal regime and turbidity currents in the hyperpycnal regime form the coarse- to fine-grained turbidite sequences. The internal sources and sinks in both the river basin and canyon conduit complicate the chronological, geochemical and sedimentary signals in the system. This is a highly complex sediment-routing system in terms of physical, geochemical, and sedimentary signals that requires an interdisciplinary approach to understand the interplay among them.

To further advance our understanding of the GPR–GPSC system or similar systems in the future, there are two challenges. The first lies in improving the observational methods for capturing passing turbidity currents in their entirety (the flow and suspended sediment structures in space and time, and the material they carry) and the corresponding signature they leave on the seafloor. The second challenge is to improve our ability to model, in a prognostic fashion, the generation (start from the plunging process of the hyperpycnal plume at the head of the canyon) and propagation of turbidity currents down the canyon, with particular attention to the processes of sediment entrainment and deposition at the flow-seabed interface, which determines the fate of the turbidity current.

Acknowledgments

All the authors are grateful to the R.O.C. Ministry of Science and Technology (formerly the National Science Council-NSC) for the financial support to the FATES research program (Fate of Terrestrial/Non-terrestrial Substances in the Kaoping Submarine Canyon, 2003–2006; Fate and Transport of Terrestrial/Non-terrestrial Substances in a Collision Margin of Arc and Continental, 2006-2009; and Fate of Terrestrial/Non-terrestrial Sediments in High Yield Particle-Export River-Sea Systems, 2009-), and to the individual authors. The authors also acknowledge the use of R/V Ocean Researcher I and III in the fieldwork, which is vital in the data acquisition and the success of the research. JTL and RHR-B benefited from the support of the NSC-DAAD (German Academic Exchange Service) Personnel Exchange Program. We benefited from discussions with Robert Sparkes. We thank Peter Talling and another anonymous reviewer and the guest editors J.P. Walsh and Patricia Wiberg for their helpful comments and suggestions to improve the manuscript.

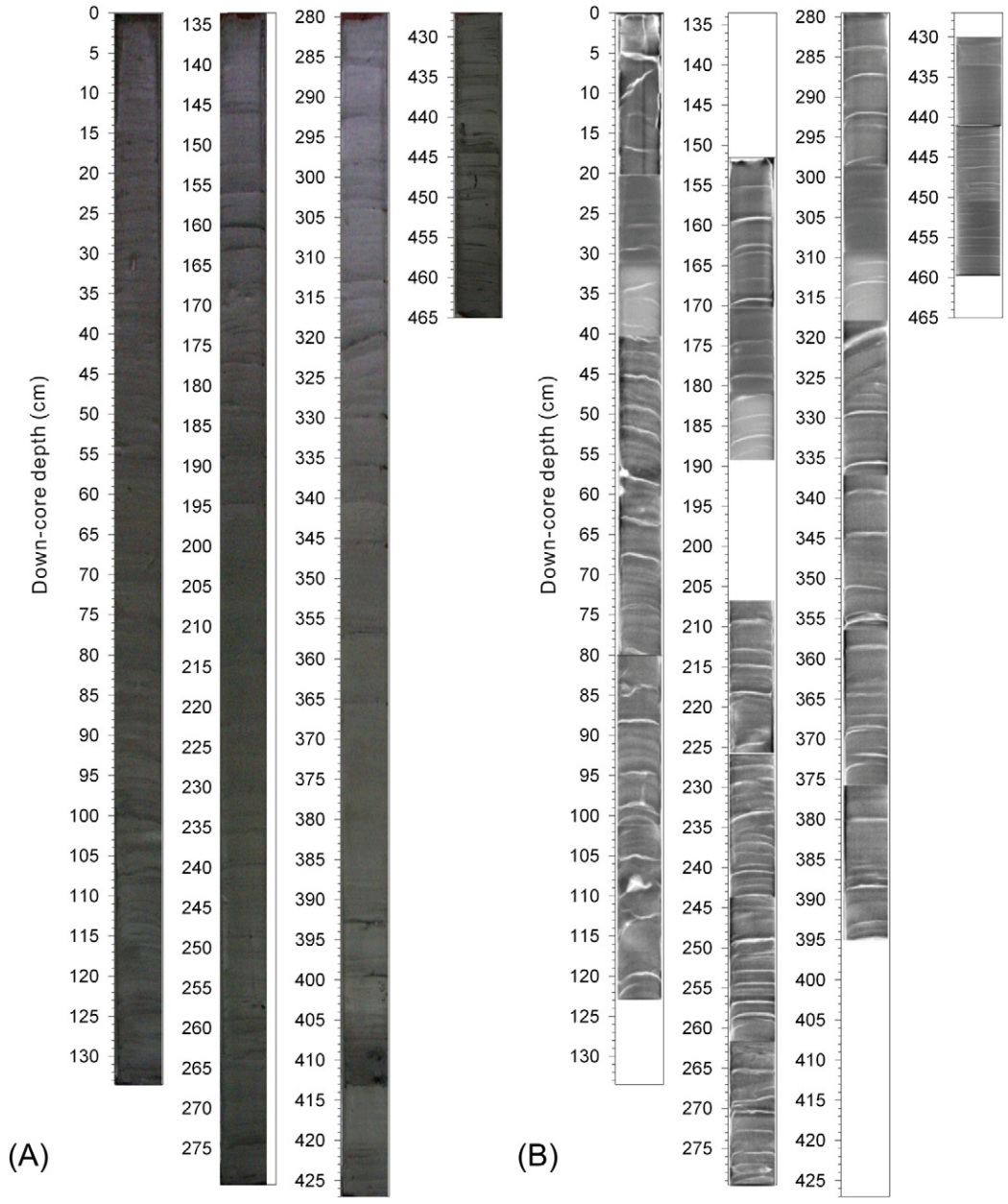

Fig. 23. Photo of Core OR1-811 K31A (A), and images of the X-ray radiograph of the segments of the core (B).

Appendix A. Supplementary data

Supplementary data associated with this article can be found in the online version, at http://dx.doi.org/10.1016/j.earscirev.2015.10.012. These data include the Google map of the most important areas described in this article.

References

Allen, P.A., 2008. From landscapes into geological history. Nature 451, 274–276. http://dx.doi.org/10.1038/nature0658.

Arzola, R.G., Russell, B.W., Lastras, G., Masso, D.G., Weaver, P.P.E., 2008. Sedimentary features and processes in the Nazaré and Setúbal submarine canyons, west Iberian margin. Mar. Geol. 250, 64–88.

Baker, E.T., Hickey, B.M., 1986. Contemporary sedimentation processes in and around an active West Coast submarine canyon. Mar. Geol. 71 (1–2), 15–34.

Bianchi, T.S., 2007. Biogeochemistry of Estuaries. Oxford University Press, New York (706 pp.).

Bianchi, T.S., Allison, M.A., 2009. Large-river delta-front estuaries as natural "recorders" of global environmental change. Proc. Natl. Acad. Sci. U. S. A. 106 (20), 8085–8092.

Blair, N.E., Leithold, E.L., Ford, S.T., Peeler, K.A., Holmes, J.C., Perkey, D.W., 2003. The persistence of memory: the fate of ancient sedimentary organic carbon in a modern sedimentary system. Geochim. Cosmochim. Acta 67, 63–73. http://dx.doi.org/10.1016/S0016-7037(02)01043-8.

Brassell, S.C., Eglinton, G., Mo, F.J., 1986. Biological marker compounds as indicators of the depositions! History of the Maoming oil shale. Org. Geochem. 10 (4–6), 927–941. http://dx.doi.org/10.1016/S0146-6380(86)80030-4.

Carlin, J.A., Dellapenna, T.M., Strom, K., Noll IV, C.J., 2015. The influence of a salt wedge intrusion on fluvial suspended-sediment and the implications for sediment transport to the adjacent coastal ocean: a study of the lower Brazos River TX, USA. Mar. Geol. 359, 134–147.

Carter, L., Milliman, J.D., Talling, P.J., Gavey, R., Wynn, R.B., 2012. Near-synchronous and delayed initiation of long run-out submarine sediment flows from a record-breaking river flood, offshore Taiwan. Geophys. Res. Lett. 39, L12603. http://dx.doi.org/10.1029/2012GL051172.

Carter, L., Gavey, R., Talling, P.J., Liu, J.T., 2014. Insights into submarine geo-hazards from breaks in the subsea telecommunication cables. Oceanography 27 (2), 58–67. http://dx.doi.org/10.5670/10.5670/oceanog.2014.40.

Chemenda, A.I., Yang, R.-K., Septhan, J.-F., Konstantinovskaya, E.A., Ivanov, G.M., 2001. New results from physical modeling of arc-continent collision in Taiwan:

evolutionary model. Tectonophysics 333, 159–178. http://dx.doi.org/10.1016/S0040-1951(00)00273-0.
Chiang, C.S., Yu, H.S., 2006. Morphotectonics and incision of the Kaoping Submarine Canyon, SW Taiwan orogenic wedge. Geomorphology 80, 199–213. http://dx.doi.org/10.1016/j.geomorph.2006.02.008.
Chiang, C.S., Yu, H.S., 2008. Evidence of hyperpycnal flows at the head of the meandering Kaoping Canyon off SW Taiwan. Geo-Mar. Lett. 28 (3), 161–169. http://dx.doi.org/10.1007/s00367-007-0098-7.
Chiang, C.S., Yu, H.S., 2011. Sedimentary erosive processes and sediment dispersal in Kaoping submarine canyon. Sci. China Earth Sci. 54 (2), 259–271. http://dx.doi.org/10.1007/s11430-010-4070-y.
Chien, F.-C., Kuo, H.-C., 2011. On the extreme rainfall of Typhoon Morakot (2009). J. Geophys. Res. 116, D05104. http://dx.doi.org/10.1029/2010JD015092.
Choi, B.-J., Wilkin, J.L., 2007. The effect of wind on the dispersal of the Hudson River plume. J. Phys. Oceanogr. 37 (7), 1878–1897.
Dachs, J., Bayona, J.M., Fowler, S.W., Miquel, J.C., Albaiges, J., 1996. Vertical fluxes of polycyclic aromatic hydrocarbons and organochlorine compounds in the western Alboran Sea (southwestern Mediterranean). Mar. Chem. 52 (1), 75–86. http://dx.doi.org/10.1016/0304-4203(95)00084-4.
Dadson, S.J., Chen, H., Dade, W.B., Hsieh, M.-L., Willett, S.D., Hu, J.-C., Horng, M.J., Chen, M.C., Stark, C.P., Lague, D., Lin, J.-C., 2003. Links between erosion, runoff variability and seismicity in the Taiwan orogen. Nature 426, 648–651. http://dx.doi.org/10.1038/nature02150.
Drexler, T.M., Nittrouer, C.A., Mullenbach, B.L., 2006. Impact of local morphology on sedimentation in a submarine canyon, rov studies in eel canyon, northern California, U.S.A. J. Sediment. Res. 76, 839–853.
Eglinton, G., Hamilton, R.J., 1967. Leaf epicuticular waxes. Science 156 (3780), 1322–1335. http://dx.doi.org/10.1126/science.156.3780.1322.
Fang, M.D., Lee, C.L., Yu, C.S., 2003. Distribution and source recognition of polycyclic aromatic hydrocarbons in the sediments of Hsin-ta Harbour and adjacent coastal areas, Taiwan. Mar. Pollut. Bull. 46 (8), 941–953. http://dx.doi.org/10.1016/S0025-326X(03)00099-7.
Fang, M.D., Hsieh, P.C., Ko, F.C., Baker, J.E., Lee, C.L., 2007. Sources and distribution of polycyclic aromatic hydrocarbons in the sediments of Kaoping river and submarine canyon system, Taiwan. Mar. Pollut. Bull. 54 (8), 1179–1189. http://dx.doi.org/10.1016/j.marpolbul.2007.04.012.
Fang, M.-D., Chang, W.-K., Lee, C.-L., Liu, J.T., 2009. The use of polycyclic aromatic hydrocarbons as a particulate tracer in the water column of Gaoping (Kaoping) Submarine Canyon. J. Mar. Syst. 76 (4), 457–467. http://dx.doi.org/10.1016/j.jmarsys.2007.08.004.
Fang, M.D., Lee, C.L., Jiang, J.J., Ko, F.C., Baker, J.E., 2012. Diffusive exchange of PAHs across the air-water interface of the Kaohsiung Harbor lagoon, Taiwan. J. Environ. Manag. 110, 179–187. http://dx.doi.org/10.1016/j.jenvman.2012.06.001.
Fox, J.M., Hill, P.S., Milligan, T.G., Boldrin, A., 2004. Flocculation and sedimentation on the Po River Delta. Mar. Geol. 203 (1–2), 95–107.
Goodbred, S.L., 2003. Response of the Ganges dispersal system to climate change: a source-to-sink view since the last interstade. Sediment. Geol. 162 (1–2), 83–104.
Hale, R., Nittrouer, C., Liu, J.T., Keil, R., Ogston, A., 2012. Effects of a major typhoon on sediment accumulation in Fangliao Canyon, SW Taiwan. Mar. Geol. 326-328, 116–130. http://dx.doi.org/10.1016/j.margeo.2012.07.008.
Harris, P.T., Wihteway, T., 2011. Global distribution of large submarine canyons: geomorphic differences between active and passive continental margins. Mar. Geol. 285, 68–86.
Hilton, R.G., Galy, A., Hovius, N., Horng, M.-J., Chen, H., 2011a. Efficient transport of fossil organic carbon to the ocean by steep mountain rivers: an orogenic carbon sequestration mechanism. Geology 39 (1), 71–74. http://dx.doi.org/10.1130/G31352.1.
Hilton, R.G., Meunier, P., Hovius, N., Bellingham, P.J., Galy, A., 2011b. Landslide impact on organic carbon cycling in a temperate montane forest. Earth Surf. Process. Landf. 36 (12), 1670–1679. http://dx.doi.org/10.1002/esp.2191.
Hsieh, M.-L., Capart, H., 2013. Late Holocene episodic river aggradation along the Laonong River (southwestern Taiwan): An application to the Tseng-wen Reservoir Transbasin Diversion Project. Eng. Geol. 159, 83–97. http://dx.doi.org/10.1016/j.enggeo.2013.03.019.
Hsieh, M.-L., Chyi, S.-J., 2010. Late Quaternary mass-wasting records and formation of fan terraces in the Chen-yeo-lan and Lao-nung catchments, central-southern Taiwan. Quat. Sci. Rev. 29, 1399–1418. http://dx.doi.org/10.1016/j.quascirev.2009.10.002.
Hsieh, M.-L., Lai, L.S.-H., Lin, C.D.-J., Bruce, J., Shyu, H., 2012. Late Quaternary landscape evolution and genesis of the 2009 catastrophic landslide in the Hsiao-lin area, southwestern Taiwan. Geomorphology 179, 225–239. http://dx.doi.org/10.1016/j.geomorph.2012.08.014.
Hsu, R.T., Liu, J.T., 2010. In-situ estimations of the density and porosity of varying sizes in a submarine canyon. Mar. Geol. 276, 105–109. http://dx.doi.org/10.1016/j.margeo.2010.07.003.
Hsu, S.-K., Sibuet, J.-C., 2004. Continent-ocean transition of the northern South China Sea and off southwestern Taiwan. Mar. Geophys. Res. 25 (1–2), 1–4. http://dx.doi.org/10.1007/s11001-005-0729-1.
Hsu, S.-K., Kuo, J., Lo, C.-L., Tsai, C.-H., Doo, W.-B., Ku, C.-Y., Sibuet, J.-C., 2008. Turbidity currents, submarine landslides and the 2006 Pingtung earthquake off SW Taiwan. Terr. Atmos. Ocean. Sci. 19, 767–772. http://dx.doi.org/10.3319/TAO.2008.19.6.767(PT).
Hsu, R.T., Liu, J.T., Su, C.-C., Kao, S.-J., Chen, S.-N., Kuo, F.-H., Huang, J.C., 2014. On the links between a river's hyperpycnal plume and marine benthic nepheloid layer in the wake of a typhoon. Prog. Oceanogr. 127, 62–73. http://dx.doi.org/10.1016/j.pocean.2014.06.001.
Huang, C.-Y., Wu, W.-Y., Chang, C.-P., Tsao, S., Yuang, P.B., Lin, C.-W., Xia, K.-Y., 1997. Tectonic evolution of accretionary prism in the arc-continent collision terrance of Taiwan. Tectonophysics 281, 31–51. http://dx.doi.org/10.1016/S0040-1951(97)00157-1.
Huang, Y.J., Lee, C.L., Fang, M.D., 2011. Distribution and source differentiation of PAHs and PCBs among size and density fractions in contaminated harbor sediment particles and their implications in toxicological assessment. Mar. Pollut. Bull. 62 (2), 432–439. http://dx.doi.org/10.1016/j.marpolbul.2010.11.022.
Huang, H.C., Lee, C.L., Lai, C.H., Fang, M.D., Lai, I.C., 2012. Transboundary movement of polycyclic aromatic hydrocarbons (PAHs) in the Kuroshio Sphere of the western Pacific Ocean. Atmos. Environ. 54, 470–479. http://dx.doi.org/10.1016/j.atmosenv.2012.02.066.
Huh, C.-A., Lin, H.-L., Lin, S., Huang, Y.-W., 2009a. Modern accumulation rates and a budget of sediment off the Gaoping (Kaoping) River, SW Taiwan: a tidal and flood dominated depositional environment around a submarine canyon. J. Mar. Syst. 76, 405–416. http://dx.doi.org/10.1016/j.jmarsys.2007.07.009.
Huh, C.-A., Liu, J.T., Lin, H.-L., Xu, J.P., 2009b. Tidal and flood signatures of settling particles in the (SW Taiwan) revealed from radionuclide and flow measurements. Mar. Geol. 267, 8–17. http://dx.doi.org/10.1016/j.margeo.2009.09.001.
Hung, J.-J., Ho, C.-Y., 2014. Typhoon- and earthquake-enhanced concentration and inventory of dissolved and particulate trace metals along two submarine canyons off southwestern Taiwan. Estuar. Coast. Shelf Sci. 136, 179–190. http://dx.doi.org/10.1016/j.ecss2013.11.004.
Hung, J.-J., Hsu, C.-L., 2004. Present state and historical changes of trace metal pollution in Kaoping coastal sediments, southwestern Taiwan. Mar. Pollut. Bull. 49, 986–998. http://dx.doi.org/10.1016/j.marpolbul.2004.06.028.
Hung, J.-J., Yang, C.-Y., Lai, I.-J., 2004. Meterologic control on physical and chemical weathering rates and material fluxes from a tropical (Kaoping) river watershed in Taiwan. Joint AOGS 1st Annual Meeting & 2nd APHW Conference, Singapore, p. 759.
Hung, J.-J., Lu, C.-T., Huh, C.-A., Liu, J.T., 2009. Geochemical controls on distributions and speciation of As and Hg in sediments along the Gaoping (Kaoping) estuary–canyon system off southwestern Taiwan. J. Mar. Syst. 76 (4), 479–495. http://dx.doi.org/10.1016/j.jmarsys.2008.03.022.
Hung, J.-J., Yeh, Y.-T., Huh, C.-A., 2012. Efficient transport of terrestrial particulate carbon in a tectonically-active marginal sea off southwestern Taiwan. Mar. Geol. 315-318, 29–43. http://dx.doi.org/10.1016/j.margeo.2012.05.006.
Jiang, J.J., Lee, C.L., Fang, M.D., Liu, J.T., 2009. Polycyclic aromatic hydrocarbons in coastal sediments of southwest Taiwan: an appraisal of diagnostic ratios in source recognition. Mar. Pollut. Bull. 58 (5), 752–760. http://dx.doi.org/10.1016/j.marpolbul.2008.12.017.
Kao, S.-J., Shiah, F.-K., Wang, C.-H., Liu, K.-K., 2006. Efficient trapping of organic southwestern Taiwan. Cont. Shelf Res. 26, 2520–2537. http://dx.doi.org/10.1016/j.csr.2006.07.030.
Kao, S.J., Dai, M., Selvaraj, K., Zhai, W., Cai, P., Chen, S.N., Yang, J.Y.T., Liu, J.T., Liu, C.C., Syvitski, J.P.M., 2010. Cyclone-driven deep sea injection of freshwater and heat by hyperpycnal flow in the subtropics. Geophys. Res. Lett. 37, L21702. http://dx.doi.org/10.1029/2010GL044893.
Kao, S.-J., Hilton, R.G., Selvaraj, K., Dai, M., Zehetner, F., Huang, J.-C., Hsu, S.-C., Sparkes, R., Liu, J.T., Lee, T.-Y., Yang, J.-Y.T., Galy, A., Xu, X., Hovius, N., 2014. Preservation of terrestrial organic carbon in marine sediments off shore Taiwan: mountain building and atmospheric carbon dioxide sequestration. Earth Surf. Dyn. 1, 127–139. http://dx.doi.org/10.5194/esurf-2-127-2014.
Kineke, G.C., Woolfe, K.J., Kuehl, S.A., Milliman, J.D., Dellapenna, T.M., Prudon, R.G., 2000. Sediment export from the Sepik River, Papua New Guinea: evidence for a divergent sediment plume. Cont. Shelf Res. 20, 2239–2266.
Kuehl S., Alexander C.R., Blair N.E., Harris C.K., Marsaglia K.M., Ogston A.S., Orpin A.R., Roering J., Bever A., Bilderback E.L., Carter L., Cerovski-Darriau C., Childress L.B., Corbett R., Hale R., Leithold E.L., Litchfield N., Moriarty J.M., Page M.J., Pierce L.E., Upton P., and Walsh J.P., A Source to Sink Perspective of the Waipaoa River Margin. (in this volume).
Kunze, E., Rosenfeld, L.K., Carter, G.S., Gregg, M.C., 2002. Internal waves in Monterey submarine canyon. J. Phys. Oceanogr. 32, 1890–1913. http://dx.doi.org/10.1175/1520-0485(2002)032<1890:IWIMSC>2.0.CO;2.
Lai, I.-C., Lee, C.-L., Zeng, K.-Y., Huang, H.-C., 2011. Seasonal variation of atmospheric polycyclic aromatic hydrocarbons along the Kaohsiung coast. J. Environ. Manag. 92 (8), 2029–2037. http://dx.doi.org/10.1016/j.jenvman.2011.03.026.
Lai, I.-C., Chang, Y.-C., Lee, C.-L., Chiou, G.-Y., Huang, H.-C., 2013. Source identification and characterization of atmospheric polycyclic aromatic hydrocarbons along the southwestern coastal area of Taiwan - with a GMDH approach. J. Environ. Manag. 115, 60–68. http://dx.doi.org/10.1016/j.jenvman.2012.11.018.
Lai, I.-C., Lee, C.-L., Ko, F.-C., Lin, R.-J., Huang, H.-C., 2014. Persistent organic pollutants in tropical coastal and offshore environment: part A: atmospheric polycyclic aromatic hydrocarbons. Int. J. Environ. Sci. Technol. 12 (3), 1075–1086. http://dx.doi.org/10.1007/s13762-013-0482-y.
Lallemand, S.E., Tsien, H.-H., 1997. An introduction to active collision in Taiwan. Tectonophysics 274, 1–4. http://dx.doi.org/10.1016/S0040-1951(96)00294-6.
Lee, I.-H., Liu, J.T., 2006. Rectification of the heading and tilting of sediment trap arrays due to strong tidal currents in a submarine canyon. Geophys. Res. Lett. 33, L08609. http://dx.doi.org/10.1029/2005GL025183.
Lee, I.-H., Lien, R.-C., Liu, J.T.*., Chuang, W.-S., 2009a. Turbulent mixing and internal tides in Gaoping (Kaoping) Submarine Canyon, Taiwan. J. Mar. Syst. 76 (4), 383–396. http://dx.doi.org/10.1016/j.jmarsys.2007.08.005.
Lee, I.-H., Wang, Y.-H., Liu, J.T., Chuang, W.-S., Xu, J.P., 2009b. Internal tidal currents in the Gaoping (Kaoping) Submarine Canyon. J. Mar. Syst. 76 (4), 397–404. http://dx.doi.org/10.1016/j.jmarsys.2007.12.011.
Lin, H.-L., Liu, J.T., Hung, G.-W., 2005. Foraminiferal shells in sediment traps: implications of biogenic particle transport in the Kao-ping Submarine Canyon. Cont. Shelf Res. 25, 2261–2272. http://dx.doi.org/10.1016/j.csr.2005.09.001.
Lin, B.S., Brimblecombe, P., Lee, C.L., Liu, J.T., 2013. Tracing typhoon effects on particulate transport in a submarine canyon using polycyclic aromatic hydrocarbons. Mar. Chem. 157, 1–11. http://dx.doi.org/10.1016/j.marchem.2013.07.004.

Liu, J.T., Lin, H.-L., 2004. Sediment dynamics in a submarine canyon: a case of river-sea interaction. Mar. Geol. 207 (1–4), 55–81. http://dx.doi.org/10.1016/j.margeo.2004.03.015.
Liu, C.-S., Huang, I.L., Teng, L.S., 1997. Structural features off southeastern Taiwan. Mar. Geol. 137, 305–319. http://dx.doi.org/10.1016/S0025-3227(96)00093-X.
Liu, J.T., Liu, K.-J., Huang, J.-S., 2002. The effect of a submarine canyon on river sediment dispersal and inner shelf sediment movements in southern Taiwan. Mar. Geol. 181, 357–386. http://dx.doi.org/10.1016/S0025-3227(01)00219-5.
Liu, J.T., Lin, H.-L., Hung, J.-J., 2006. A submarine canyon conduit under typhoon conditions off Southern Taiwan. Deep-Sea Res. I 53, 223–240. http://dx.doi.org/10.1016/j.dsr.2005.09.012.
Liu, J.P., Liu, C.S., Xu, K.H., Milliman, J.D., Chiu, J.K., Kao, S.J., Lin, S.W., 2008. Flux and fate of small mountainous rivers derived sediments into the Taiwan Strait. Mar. Geol. 256, 65–76. http://dx.doi.org/10.1016/j.margeo.2008.09.007.
Liu, J.T., Hung, J.-J., Huang, Y.-W., 2009a. Partition of suspended and riverbed sediments related to the salt-wedge in the lower reaches of a small mountainous river. Mar. Geol. 264, 152–164. http://dx.doi.org/10.1016/j.margeo.2009.05.005.
Liu, J.T., Huh, C.-A., You, C.-F., 2009b. Fate of terrestrial substances in the Gaoping (Kaoping) shelf/slope and in the off SW Taiwan. J. Mar. Syst. 76 (4), 367–368. http://dx.doi.org/10.1016/j.jmarsys.2008.08.005.
Liu, J.T., Hung, J.-J., Lin, H.-L., Huh, C.-A., Lee, C.-L., Hsu, R.T., Huang, Y.-W., Chu, J.C., 2009c. From Suspended Particles to Strata: The Fate of Terrestrial Substances in the Gaoping (Kaoping) Submarine Canyon. J. Mar. Syst. 76 (4), 417–432. http://dx.doi.org/10.1016/j.jmarsys.2008.01.010.
Liu, J.T., Wang, Y.-H., Lee, I.-H., Hsu, T.R., 2010. Quantifying tidal signatures of the benthic nepheloid layer in in southern Taiwan. Mar. Geol. 271, 119–130. http://dx.doi.org/10.1016/j.margeo.2010.01.016.
Liu, J.T., Wang, Y.-H., Yang, R.J., Hsu, R.T., Kao, S.-J., Lin, H.-L., Kuo, F.H., 2012. Cyclone-induced hyperpycnal turbidity currents in a submarine canyon. J. Geophys. Res. 117, C04033. http://dx.doi.org/10.1029/2011JC007630.
Liu, J.T., Kao, S.-J., Huh, C.-A., Hung, C.C., 2013. Gravity flows associated with floods and carbon burial: Taiwan as instructional source area. Annu. Rev. Mar. Sci. 5, 47–68. http://dx.doi.org/10.1146/annurev-marine-121,211-172,307.
Liu, Z., Zhao, Y., Colin, C., Stattegger, K., Wiesner, M.G., Huh, C.-A., Zhang, Y., Xiajing Li, X., Sompongchaiyakul, P., You, C.-F., Huang, C.-Y., Liu, J.T., Siringan, F.P., Le, K.P., Sathiamurthy, E., Hantoro, W.S., Liu, J., Tuo, S., Zhao, S., Zhou, S., He, Z., Wang, Y., Bunsomboonsakul, S., Li, Y., 2015. Source-to-sink processes of fluvial sediments in the South China Sea (this volume).
Lopez-Fernandez, P., Calafat, A., Sanchez-Vidal, A., Canals, M., Mar Flexas, M., Cateura, J., Company, J.B., 2013. Multiple drivers of particle fluxes in the Blanes submarine canyon and southern open slope: Results of a year round experiment. Prog. Oceanogr. 118, 95–107.
Marsaglia, K.M., DeVaughn, A.M., James, D.E., Marden, M., 2010. Provenance of fluvial terrace sediments within theWaipaoa sedimentary system and their importance to New Zealand source-to-sink studies. Mar. Geol. 270 (1–4), 84–93.
Milliman, J.D., Kao, S.-J., 2005. Hyperpycnal discharge of fluvial sediment to the ocean: impact of super-typhoon Herb (1996) on Taiwanese rivers. J. Geol. 113, 503–516.
Milliman, J.D., Syvitski, J.P.M., 1992. Geomorphic/tectonic control of sediment discharge to the ocean: The importance of small mountainous rivers. J. Geol. 100, 525–544.
Nittrouer, C.A., DeMaster, D.J., 1996. The Amazon shelf setting: Tropical, energetic, and influenced by a large river. Cont. Shelf Res. 16 (5–6), 553–573.
Page, D.S., Boehm, P.D., Douglas, G.S., Bence, A.E., Burns, W.A., Mankiewicz, P.J., 1999. Pyrogenic polycyclic aromatic hydrocarbons in sediments record past human activity: A case study in Prince William Sound, Alaska. Mar. Pollut. Bull. 38 (4), 247–260. http://dx.doi.org/10.1016/S0025-326X(98)00142-8.
Palanques, A., El Khatab, M., Puig, P., Masqué, P., Sánchez-Cabeza, J.A., Isla, E., 2005. Downward particle fluxes in the Guadiaro submarine canyon depositional system (northwestern Alboran Sea), a river flood dominated system. Mar. Geol. 220 (1–4), 23–40.
Parra, J.G., Marsaglia, K.M., Rivera, K.S., Dawson, S.T., Walsh, J.P., 2012. Provenance of sand on the Poverty Bay shelf, the link between source and sink sectors of the Waipaoa River sedimentary system. Sediment. Geol. 280, 208–233.
Pendoley, K., 1992. Hydrocarbos in Rowley Shelf (Western Australia) oysters and sediments. Mar. Pollut. Bull. 24 (4), 210–215. http://dx.doi.org/10.1016/0025-326X(92)90532-B.
Powell, T.G., Mokirdy, D.M., 1973. The effect of source material, rock type and diagenesis on the n-alkane content of sediments. Geochim. Cosmochim. Acta 37 (3), 623–633. http://dx.doi.org/10.1016/0016-7037(73)90223-8.
Powell, T.G., Foscolos, A.E., Gunther, P.R., Snowdon, L.R., 1978. Diagenesis of organic matter and fine clay minerals: a comparative study. Geochim. Cosmochim. Acta 42 (8), 1181–1197. http://dx.doi.org/10.1016/0016-7037(78)90113-8.
Prokoph, A., Adamowski, J., Adamowski, K., 2012. Influence of the 11 year solar cycle on annual streamflow maxima in Southern Canada. J. Hydrol. 442, 55–62. http://dx.doi.org/10.1016/j.jhydrol.2012.03.038.
Puig, P., Palanques, A., Martin, T., 2014. Contemporary sediment-transport processes in submarine canyons. Annu. Rev. Mar. Sci. 6, 53–77. http://dx.doi.org/10.1146/annurew-marine-010213-135037.
Rendle-Buehring, R., Steinke, S., Liu, J.T., Lin, H.-L., 2008. The effects of paleoclimatic change on sediment fluxes in the vicinity of the Gao-Ping submarine canyon, Taiwan. Geochim. Cosmochim. Acta 72 (12), A787 (Goldschmidt Conference Abstracts).
Rendle-Buehring, R., Steinke, S., Liu, J.T., Lin, H.-L., 2009. Initial sedimentological findings for 3 proximal to distal located cores in the system. Taiwanconference program and Abstracts Vol., International Symposium on Sediment Transport and Sedimentation on Asian Continental Margins, Kaohsiung, Taiwan, p. 52.
Saito, Y., Yang, Z.S., Hori, K., 2001. The Huanghe (Yellow River) and Changjiang (Yangtze River) deltas: a review on their characteristics, evolution and sediment discharge during the Holocene. Geomorphology 41 (2–3), 219–231.
Sato, K., Li, H., Tanaka, Y., Ogawa, S., Iwasaki, Y., Takami, A., Hatakeyama, S., 2008. Long-range transport of particulate polycyclic aromatic hydrocarbons at Cape Hedo remote island site in the East China Sea between 2005 and 2008. J. Atmos. Chem. 61 (3), 243–257. http://dx.doi.org/10.1007/s10874-009-9135-4.
Savinov, V.M., Savinova, T.N., Carroll, J., Matishov, G.G., Dahle, S., Naes, K., 2000. Polycyclic aromatic hydrocarbons (PAHs) in sediments of the White Sea, Russia. Mar. Pollut. Bull. 40 (10), 807–818. http://dx.doi.org/10.1016/S0025-326X(00)00004-7.
Sequeiros, O.E., Naruse, H., Endo, N., Garcia, M.H., Parker, G., 2009. Experimental study on self-accelerating turbidity currents. J. Geophys. Res. 114, C05025. http://dx.doi.org/10.1029/2008JC005149.
Shanmugam, G., 2006. Deep-Water Processes and Facies Models: Implications for Sandstone Petroleum Reservoirs. Elsevier B.V., Amsterdam, The Netherlands.
Sobarzo, M., Figueroa, M., Djurfeldt, L., 2001. Upwelling of subsurface water into the rim of the Biobio submarine canyon as a response to surface wind. Cont. Shelf Res. 21, 279–299.
Sparkes, R., 2012. Marine Sequestration of Particulate Organic Carbon from Mountain Belts Doctoral Dissertation University of Cambridge (286 pp.).
Sparkes, R.B., Lin, I.-T., Hovius, N., Galy, A., Liu, J.T., Xu, X., Yang, R., 2015. Redistribution of multi-phase particulate organic carbon in a marine shelf and canyon system during an exceptional river flood: effects of Typhoon Morakot on the GPR-Canyon system. Mar. Geol. 363, 191–201.
Su, C.-C., Tseng, J.-Y., Hsu, H.-H., Chiang, C.-S., Yu, H.-S., Lin, S., Liu, J.T., 2012. Records of submarine natural hazards off SW Taiwan. Geol. Soc. Lond., Spec. Publ. 361, 41–60. http://dx.doi.org/10.1144/SP361.5.
Talling, P.J., 2014. On the trigger, resulting flow types and frequencies of subaqueous sediment density flows in different settings. Mar. Geol. 352, 155–182.
Talling, P.J., Paull, C.K., Piper, D.J.W., 2013. How are subaqueous sediment density flows triggered, what is their internal structure and how does it evolve? Direct observations from monitoring of active flows. Earth Sci. Rev. 125, 244–287. http://dx.doi.org/10.1016/j.earscirev.2013.07.005.
Traykovski, P., Wiberg, P.L., Geyer, W.R., 2007. Observations and modeling of wave-supported sediment gravity flows on the Po prodelta and comparison to prior observations from the Eel shelf. Cont. Shelf Res. 27 (3–4), 375–399.
Tsou, C.-Y., Feng, Z.-Y., Chigira, M., 2011. Catastrophic landslide induced by Typhoon Morakot, Shiaolin, Taiwan. Geomorphology 127, 166–178. http://dx.doi.org/10.1016/j.geomorph.2010.12.013.
van Weering, T.C.E., de Stigter, H.C., Boer, W., de Haas, H., 2002. Recent sediment transport and accumulation on the NW Iberian margin. Prog. Oceanogr. 52, 349–371.
Verlaan, P.A.J., 2000. Marine *vs* fluvial bottom mud in the Scheldt Estuary. Estuar. Coast. Shelf Sci. 50, 627–638.
Walsh, J.P., Nittrouer, C.A., 2009. Understanding fine-grained river-sediment dispersal on continental margins. Mar. Geol. 263 (1), 34–45.
Wang, Y.J., Su, Y.J., 2013. Influence of solar activity on breaching, overflowing and course-shifting events of the Lower Yellow River in the late Holocene. The Holocene 23 (5), 656–666. http://dx.doi.org/10.1177/0959683612467481.
Wang, Y.H., Lee, I.H., Liu, J.T., 2008. Observation of internal tidal currents in the Kaoping Canyon off southwestern Taiwan. Estuar. Coast. Shelf Sci. 80 (1), 153–160. http://dx.doi.org/10.1016/j.ecss.2008.07.016.
Warrick, J.A., 2014. Eel River margin source-to-sink sediment budgets: Revisited. Mar. Geol. 351, 25–37.
Wu, Y., Zhang, J., Liu, S.M., Zhang, Z.F., Yao, Q.Z., Hong, G.H., Cooper, L., 2007. Sources and distribution of carbon within theYangtze River system. Estuar. Coast. Shelf Sci. 71 (1–2), 13–25.
Xu, J.P., Noble, M., Eittreim, S.L., Rosenfeld, L.K., Schwing, F.B., Pilskaln, C.H., 2002. Distribution and transport of suspended particulate matter in Monterey Canyon, California. Mar. Geol. 181, 215–234. http://dx.doi.org/10.1016/S0025-3227(01)00268-7.
Yeh, Y.-C., Shen, T.-F., Liu, S.-Y., Yang, S.-Y., Yang, Y., Kuo, F., 2013. Seafloor morphology and slope failures of the Kaoping Canyon upstream area. Promotion and Review of The Executive Yuan Program on Applying Science and Technology for Disaster Reduction, 2012 Report by Taiwan Ocean Research Institute, Kaohsiung, Taiwan.
Yu, H.-S., 2004. An under-filled foreland basin in the northern South China Sea off southwest Taiwan: incipient collision and foreland sedimentation. in: Continent–Ocean Interactions Within East Asian Marginal Seas. In: Clift, P., Kuhnt, W., Wang, P., Hayes, D. (Eds.), Geophysical Monograph Series 149. American Geophysical Union, Washington, D.C., pp. 159–173. http://dx.doi.org/10.1029/149GM09.
Yu, H.-S., Auster, P.J., Cooper, R.A., 1993. Surface geology and biology at the head of Kaoping canyon off southwestern Taiwan. Terr. Atmos. Ocean. Sci. 4 (4), 441–455.
Yu, H.S., Chiang, C.S., Shen, S.M., 2009. Tectonically active sediment dispersal system in SW Taiwan margin with emphasis on the Kaoping Submarine Canyon. J. Mar. Syst. 76 (4), 369–382. http://dx.doi.org/10.1016/j.jmarsys.2007.07.010.
Yunker, M.B., Macdonald, R.W., Vingarzan, R., Mitchell, R.H., Goyette, D., Sylvestre, S., 2002. PAHs in the Fraser River basin: a critical appraisal of PAH ratios as indicators of PAH source and composition. Org. Geochem. 33 (4), 489–515. http://dx.doi.org/10.1016/S0146-6380(02)00002-5.